Weakly correlated electrons on a square lattice: Renormalization-group theory

D. Zanchi*

Institut für Theoretische Physik der Freien Universität Berlin, Arnimallee 14, 14195 Berlin, Germany

H. J. Schulz[†]

Laboratoire de Physique des Solides, Université Paris-Sud, 91405 Orsay, France

We formulate the exact Wilsonian renormalization group for a system of interacting fermions on a lattice. The flow equations for all vertices of the Wilson effective action are expressed in the form of the Polchinski equation. The advantage of this renormalization scheme is that the flow itself has a physical interpretation, i.e., the cutoff has the meaning of the temperature. We apply this method to the Hubbard model on a square lattice using both zero- and finite-temperature methods. Truncating the effective action at the sixth term in fermionic variables and neglecting self-energy renormalization, we obtain the one-loop functional renormalization equations for the effective interaction. We find the temperature of the instability T_c^{RG} as a function of doping. Furthermore we calculate the renormalization of the angle-resolved correlation functions for the superconductivity (SC) and for the antiferromagnetism (AF). The dominant component of the SC correlations is of the type $d_{x^2-y^2}$, while the AF fluctuations are of the type s. Following the strength of both SC and AF fluctuations along the instability line, we obtain the phase diagram. The temperature T_c^{RG} can be identified with the crossover temperature T_{co} found in the underdoped regime of the high-temperature superconductors, while in the overdoped regime T_c^{RG} corresponds to the superconducting critical temperature.

I. INTRODUCTION

In systems of correlated fermions on a lattice some interesting and also puzzling physics seems to happen when interaction-induced localization tendencies, antiferromagnetic fluctuations, and superconducting fluctuations are mixed. The standard example of such a system is copper-oxide superconductors.[1] In the underdoped regime, between the antiferromagnetic (AF) and superconductivity (SC) phases, correlations of both AF and SC types are strongly enhanced, and a pseudogap is visible in the one-particle spectrum and in the spin response functions. The pseudogap regime is limited from above by a crossover temperature $T_{co}(x)$, a monotonously decreasing function of doping. At the temperatures $T \gtrsim T_{co}$ the underdoped materials are ''strange metals'': many physical properties are unlike those of a standard Fermi liquid.[2] In the overdoped regime $T_{co}(x)$ merges with the critical temperature for superconductivity, and the regime $T > T_c$ is merely a Fermi liquid. Another interesting feature of the phase diagram is the unusual form of the order parameter. After a rather long period of controversies the $d_{x^2-y^2}$ symmetry is finally generally accepted.[3,4] This is one of the reasons to believe that the pairing mechanisms are tightly related to the antiferromagnetic tendencies and not to the standard phonon-exchange mechanisms. The $d_{x^2-y^2}$ form of the superconducting correlations also subsists in the pseudogap regime, as seen in recent angle-resolved photoemission[5] and tunneling[6] experiments. The simultaneous existence of strong AF correlations, as seen by NMR[7] or neutron-scattering[8] experiments, and even localization tendencies such as the flattening of the band,[4] make us conclude that the interpretation of this regime in terms of only superconducting or antiferromagnetic fluctuations is not sufficient, especially because we expect that they are coupled.

It is striking that some other apparently completely different systems of correlated fermions have very similar properties. A phase diagram with the superconducting phase in the vicinity of the spin density wave (i.e., antiferromagnetic) instability also characterizes the quasi-one-dimensional Bechgaard salts[9] and the quasi-two-dimensional organic superconductors of the ET family,[10] where instead of doping the relevant parameter for the phase diagram is pressure. However the common feature of all these compounds is that they are systems of correlated fermions with reduced dimensionality ($D < 3$), and with strongly anisotropic and more or less nested Fermi surfaces. The main points for the understanding of the three groups of compounds are (i) the destruction of the nesting by doping (cuprates) or by applying pressure (Bechgaard salts and ET); and (ii) the suppression of the umklapp processes by doping the half-filled band (in the cuprates and ET's) or by making the half–filled band effectively quarter-filled through the breaking of the longitudinal dimerization by pressure (in the Bechgaard salts). Concerning the Bechgaard salts it is interesting to remark that some recent interpretations of the phase diagram of the (TMTSF)PF$_6$ material[11] suggest that the intermediate regime between the high-temperature one-dimensional (1D) behavior and the low-temperature 3D physics is a strange 2D liquid with properties very similar to those of the underdoped cuprates above the crossover temperature T_{co}.

From the theoretical point of view it is certainly interesting to construct a theory able to treat antiferromagnetic and superconducting tendencies in more than one dimension on the same footing, and to follow how the result changes with some external parameter that destroys nesting and the Mott-like localization. The first question one can ask is whether a purely repulsive model like, for example, the Hubbard model (or some generalization of it) contains coexisting and inter-

dependent antiferromagnetic and superconducting correlations. In such a model the antiferromagnetic fluctuations are associated with the enhancement of the particle-hole (p-h) propagators at low energies, and the superconducting tendencies appear through particle-particle (p-p) propagators. The Hubbard model is appropriate because at half-filling a simple mean-field calculation already gives an antiferromagnetic instability at a finite temperature. However, if one also tries to include the p-p processes, the problem becomes nontrivial even in the weak-coupling limit: a simple mean-field theory is not able to follow both p-h and p-p correlation channels. One can of course try to remedy this problem by including summation of selected subseries of higher-order diagrams. One such attempt was to calculate the effective Cooper amplitude as a sum of bubble and ladder random-phase-approximation (RPA) series.[12,13] The resulting Cooper amplitude is then used as coupling constant for assumed effective BCS theory. This procedure thus explicitly decouples three different summations (RPA bubbles, RPA ladder, and BCS ladder) without real justification. FLEX (conserving) calculations[14] based on similar simplifications are also prejudiced by the choice of diagrams to be summed. The only way to proceed systematically is to construct a renormalization group that takes into account all p-p and p-h loops of a given order (or to use the equivalent parquet approach). In (quasi-) one dimension, the renormalization group has been successfully used, and is one of the basic theoretical ingredients in the physics of low-dimensional metals.[9,15,16]

In two dimensions only a limited number of simplified cases was solved by the renormalization group. The poor man's scaling applied only to interactions between electrons placed at the van Hove points gives an antiferromagnetic instability at half-filling and a superconductivity of $d_{x^2-y^2}$ symmetry if the deviation of the chemical potential μ from its value at half-filling becomes of the order of the critical temperature of the antiferromagnetic state.[17,18] The equivalent parquet approach has been used for half-filling (but without the limitation to the van Hove points), and also produces an antiferromagnetic instability.[19,20] Parquet calculations for simple flat Fermi surfaces[21] give an antiferromagnetic instability, but cannot provide a continuous phase diagram as a function of some imperfect nesting parameter or band filling: the $d_{x^2-y^2}$-like superconducting pole appears simply by cutting the p-h part of the flow, as in Ref. 17. A scaling approach to a system with a Fermi surface with both flat and curved parts[22] has also reported a superconducting instability in a purely repulsive model, together with deviations from Fermi-liquid behavior. However, a complete one-loop renormalization group (or parquet) for a real *band* of electrons with imperfect and tunable nesting, or doping, still remains unresolved. The main difficulty is related to the correct treatment of the coupling between p-p and p-h channels.

Different authors have tried to avoid taking into account the coupling between the different renormalization channels, making drastic simplifications or limiting themselves to some particular forms of the Fermi surfaces or only to the low-energy effective action. In our former publications[23,24] we have shown that in the Hubbard model one can treat the p-h channel perturbatively if the filling is sufficiently far

from one-half. Then the renormalization group gives only a weak Kohn-Luttinger-like pairing. The p-p part of the flow is decoupled from the p-h one in the low-energy regime for the simple reason that the p-h part is negligible there. Other calculations based on the perturbative treatment of the p-h channel were also reported.[25,26] If the Fermi surface is well (but imperfectly) nested, and this is exactly the interesting regime, this strategy does not work any longer because both p-p and p-h loops are nonperturbatively large, even for weak interactions. In the case of the square Fermi surface (with or without the van Hove singularities) taking only the leading logarithmic part the coupling between the channels into account[27] is equally insufficient. Another way to proceed is to see the 2D Hubbard system as an ensemble of coupled chains.[28] This approach gives a phase diagram with superconductivity formed by pairs of electrons on different chains, giving rise to a spatially anisotropic version of a d-wave order parameter. Among the number of theoretical approaches to the Hubbard model other than via the loop summations, Monte Carlo calculations in principle take ''everything'' into account, but it is still unclear whether they give[29] the superconductivity or not.[13,30]

In the present paper we seek to reliably determine the phase diagram of the Hubbard model in the vicinity of half-filling, where p-h processes are nonperturbatively enhanced and at least nearly as important as p-p ones. We also detect the dominant components of the angle-resolved correlation functions for antiferromagnetism and superconductivity as functions of temperature. This allows us to know the symmetry of the microscopic fields whose fluctuations become important. The method that we will use is a generalization of Shankar's renormalization-group approach[31] to an arbitrary form of the Fermi surface. In particular, the Kadanoff-Wilson mode elimination (developed by Shankar for 2D fermions) applied to the effective action with only two-particle interaction retains only strictly logarithmic contributions to the flow. Thus, even if the nesting is very good but not perfect, the p-h part of the flow would be zero because the logarithmic singularity is destroyed by imperfect nesting. To keep the p-h part of the flow finite even in the case of imperfect nesting, we start by formulating the *exact* Kadanoff-Wilson-Polchinski renormalization group for fermions on a lattice. This was formulated previously[32,33] only for quantum fields with *one* zero-energy point in the momentum space, like the ϕ^4 field theory (critical phenomena). In many-fermion systems in more than one dimension we have, on the contrary, a whole Fermi surface that plays the role of a zero energy manifold, which makes the calculations more complicated. Starting with the full bandwidth as the initial energy cutoff we perform an iterative mode elimination, reducing the cutoff Λ around the Fermi surface. Collecting at each step of the renormalization all the terms (cumulants) of the effective action, we obtain the Polchinski equation for the vertices of the effective theory at a given step of the renormalization. It is important that even if the initial interaction is only a four-point function (two-particle interaction), vertices of *all* higher orders are created by the renormalization procedure. Once the exact renormalization group is formulated we proceed with its truncation at the one-loop level: the one-loop truncation of the flow for the four-point vertex is done by neglecting all renormalization-group-created verti-

ces of order larger than 6. Shankar[31] already remarked that the six-point function created by the mode elimination is essential to obtain a nonlogarithmic contribution to the four-point vertex (the effective interaction). The one-loop renormalization of the interaction that we obtain in this way appears to be generally *nonlocal* in Λ, i.e., the flow of the vertex at a given step of the renormalization depends on the values of the vertex at former steps. This is certainly not pleasant, but is (as far as we can see) a necessary property of the Kadanoff-Wilson-Polchinski (KWP) procedure if we want to keep more than just purely logarithmic contributions. In principle, some other renormalization-group (RG) schemas, local in Λ, could also be used. In particular, the field-theory scheme,[23] also derived recently from an exact Polchinski RG equation,[34] or, on the other hand, Morris' version of one-particle-irreducible (1PI) RG's, are procedures[33] local in Λ and could take into account everything what takes KWP approach. The difference between the KWP and FT approaches is that in the former the cutoff has a physical meaning. At some step of the renormalization the KWP procedure gives an effective model renormalized only by electrons with an energy $|\xi| > \Lambda$. This means that Λ acts as an energy resolution: the vertices of the model have the meaning of correlation functions energy resolved for energies larger than Λ. In fact, this is equivalent to saying that Λ acts like an effective temperature. The FT approach does not have this advantage, and one can compare it with KWP results only in the fixed point ($\Lambda \to 0$). On the other hand, Morris' 1PI equations are not suitable for the approximations that we make in our calculations. Essentially these consist of neglecting all energy dependences of the effective interaction for $|\xi| < \Lambda$, using power counting. In the KWP scheme this approximation is always allowed because, by the definition of the Wilson effective action, all electrons live in the region $|\xi| < \Lambda$ of the phase space. The approximation is not straightforward in 1PI equations, because there the ''classical'' fields are not constrained in phase space to only $|\xi| < \Lambda$, so that power counting cannot be done simply.

We apply the one-loop KWP renormalization group to the Hubbard model. One further approximation we make is to consider the effective interaction as a function only of the projection of the momenta to the square Fermi surface (marginal interactions), while the radial dependence and dynamics are neglected because they are irrelevant with respect to the Fermi-liquid scaling.[31] We also neglect the renormalization of the self-energy. If we take only marginal interactions into account this is justified at the one-loop level because the renormalizations of the weight and of the lifetime of the electrons receive nonzero contributions only at the two-loop level. We thus renormalize only the interaction $U(\theta_1, \theta_2, \theta_3)$, a function of three angular variables corresponding to the angular parts of the three external momenta, the fourth being determined by momentum conservation. We allow the θ variables to be anywhere on the almost square Fermi surface, and not only in the configurations that give perfect nesting or zero center-of-mass momentum: these two classes of the configurations would correspond only to the processes with the leading logarithmic renormalization in the p-h and p-p channels, respectively. As will become clear later, taking all three θ variables without constraints is the essential point of the calculation, because the coupling be-

tween p-p and p-h channels appears mostly through interactions that have other than just leading-logarithmic flow. This is a special feature of the square or almost square Fermi surface, and can be handled only by nonlocal (outer-shell) contributions to the flow, using the Polchinski equation.

The first aim of our calculation is to find the temperature (scale) at which the flow diverges toward strong coupling. We associate this temperature with a mean-field-like critical temperature and call it T_c^{RG}. A typical mean-field theory is then regularized for $T < T_c$ by adding counterterms that contain fermions bilinearly coupled to some order parameter. In our theory the order parameter is not known *a priori*: it is determined by the manner in which the *function* $U(\theta_1, \theta_2, \theta_3)$ diverges at $T = T_c^{RG}$. We perform a detailed analysis of the behavior of the angle-resolved correlation functions for antiferromagnetism and superconductivity, and obtain the type and the symmetry of the order parameter determining the dominant correlations near T_c^{RG}. The final result is the analog of a mean-field phase diagram of the Hubbard model. Let us focus briefly on this point. T_c^{RG} is the temperature at which the effective interactions between electrons diverge. Interpretation of this temperature as a mean-field-like critical temperature is well established in the physics of correlated fermions. For example, the divergence of the one-loop flow of a vertex with a total momentum equal to zero is nothing but the BCS critical point.[31] Another example is the theory of the spin-density-wave phases in quasi-one-dimensional organic conductors.[35] Here the basic concept is the analysis of the divergence of the RPA vertex near the $2k_F$ momentum transfer. In the language of the renormalization group the RPA theory is just one-loop renormalization in the electron-hole channel. Altogether, the divergence of the vertex at some critical temperature (scale) is indeed a breakdown of the renormalization procedure, but with a precise physical interpretation.

We are considering a two-dimensional system, another reason to be careful about the interpretation of T_c^{RG}: in the case of magnetism, this indicates the onset of well-defined finite-range correlations. For weak interactions, this is typically a very well-defined crossover.[36] In the case of pairing T_c^{RG} can be identified with the onset of quasi-long-range order. However, in real systems like copper oxides even a weak interplane two-particle hopping (particle-hole-pair hopping for antiferromagnetism, or Josephson tunneling for superconductivity) stabilizes a 3D long-range order. Of course, in that case the value of the critical temperature depends on the way the planes are coupled, but that kind of analysis is out of the frame of this paper. What we do is to explore in detail the in-plane mechanisms necessary (but not sufficient) for antiferromagnetic or/and superconducting long-range order. From the point of view of single electrons, T_c^{RG} is the temperature of the onset of strong correlations that destroy one-particle coherence. Consequently, the regime $T \lesssim T_c^{RG}$ is not a Fermi liquid: the Fermi surface is destroyed by a (pseudo)gap.

In Sec. II we begin by the formulation of the many-fermion system on a lattice in terms of functional integrals. We introduce the concept of effective action, and show how it can be formally calculated using the partial trace technique. We then derive the Kadanoff-Wilson-Polchinski exact

renormalization group as one possible strategy for calculating the effective action in terms of the renormalization group flow of all vertices. Truncating the effective action at the level of sixth-order vertices, we obtain one-loop renormalization-group equations for the effective interaction and for the self-energy. In Sec. III we apply the zero-temperature one-loop renormalization group to the Hubbard model on a square lattice. This section is in fact the extended version of our recent paper.[37] We derive the flow equations for the effective interaction function and for the angle-resolved correlation functions of superconducting and anti-ferromagnetic types. After discretization of the angle θ on the Fermi surface, we numerically integrate the flow, and present the resulting phase diagram. In Sec. IV we introduce finite temperature explicitly into the renormalization-group equations. We then calculate the fixed-point values of the correlation functions at temperatures near the instability. Conclusions are given in Sec. V.

II. FORMULATION OF THE RENORMALIZATION GROUP FOR A MANY-FERMION PROBLEM ON A LATTICE

The simplest model for interacting fermions on a two-dimensional square lattice is the Hubbard Hamiltonian

$$H = -t \sum_{\langle i,j \rangle, \sigma} (a_{i,\sigma}^\dagger a_{j,\sigma} + a_{j,\sigma}^\dagger a_{i,\sigma}) + \frac{U_0}{2} \sum_i n_i n_i - \mu \sum_i n_i, \tag{2.1}$$

where $a_{i,\sigma}$ ($a_{i,\sigma}^\dagger$) is the creation (annihilation) operator of an electron at site i with spin σ, t is the intersite transfer integral, μ is the chemical potential, and U_0 is the on-site Coulomb repulsion. After Fourier transform, the Hamiltonian is written

$$H = \sum_{\sigma \mathbf{k}} \xi_{\mathbf{k}} a_{\sigma \mathbf{k}}^\dagger a_{\sigma \mathbf{k}}$$
$$+ \frac{1}{2} \sum_\sigma \sum_{\mathbf{k}_1, \mathbf{k}_2, \mathbf{k}_3} U_0 a_{-\sigma, \mathbf{k}_1 + \mathbf{k}_2 - \mathbf{k}_3}^\dagger a_{-\sigma \mathbf{k}_2} a_{\sigma \mathbf{k}_3}^\dagger a_{\sigma \mathbf{k}_1}, \tag{2.2}$$

where

$$\xi_{\mathbf{k}} = -2t(\cos k_x + \cos k_y) - \mu, \tag{2.3}$$

and the momenta are within the first Brillouin zone. In this section we want to derive the renormalization group for a more general problem. For that purpose we allow $\xi_{\mathbf{k}}$ to have a general dependence on $\mathbf{k}$. Furthermore, we suppose that the interaction can be nonlocal and dynamical; that is, we suppose that it depends on energies and momenta of the interacting particles.

The statistical mechanics of souch general model is given by the partition function[31]

$$Z = \int \mathcal{D}\bar{\Psi} \, \mathcal{D}\Psi \, e^{S\{\Psi\}}, \tag{2.4}$$

where the functional integration is over Grassmann variables $\bar{\Psi}$ (Ψ) for all electrons in the Brillouin zone. The action S is given by

$$S\{\Psi\} = S_0\{\Psi\} + S_I\{\Psi\} = T \sum_{\omega_n} \sum_{\sigma \mathbf{k}} \bar{\Psi}_{\sigma K}(i\omega_n - \xi_{\mathbf{k}})\Psi_{\sigma K}$$
$$+ \frac{1}{2} \sum_{\sigma \sigma'} T^3 \sum_{\omega_{n_1}, \omega_{n_2}, \omega_{n_3}} \sum_{\mathbf{k}_1, \mathbf{k}_2, \mathbf{k}_3}$$
$$\times U_0(K_1, K_2, K_3) \bar{\Psi}_{\sigma K_3} \bar{\Psi}_{\sigma' K_4} \Psi_{\sigma' K_2} \Psi_{\sigma K_1}. \tag{2.5}$$

The variables $\bar{\Psi}$ (Ψ) are labeled by the energy-momentum vector $K = (\omega_n, \mathbf{k})$. $\xi_{\mathbf{k}}$ is the bare spectrum measured from the Fermi level,

$$\xi_{\mathbf{k}} = \epsilon_{\mathbf{k}} - \mu,$$

where $\epsilon_{\mathbf{k}}$ is the band dispersion and μ the chemical potential. The energies and momenta are conserved so that $K_4(K_1, K_2, K_3) = (\omega_{n_1} + \omega_{n_2} - \omega_{n_3}, \mathbf{k}_1 + \mathbf{k}_2 - \mathbf{k}_3)$. We will remember that momenta are conserved up to reciprocal-lattice vectors. $U_0(K_1, K_2, K_3)$ is the most general spin-independent interaction, a function of the frequencies and momenta. The derivation of action (2.5) for a general model is equivalent to the derivation for the Hubbard model,[38,39] provided that we put $U_0(K_1, K_2, K_3)$ instead of the constant U_0 and keep $\xi_{\mathbf{k}}$ general.

We want to derive the low energy effective action (LEEA) for this model. The low-energy modes are the electronic degrees of freedom close to the Fermi surface. We will use this criterion and use the energy variable $\xi_{\mathbf{k}}$ to discriminate fast (high-energy) modes $\Psi_>$ from the slow (low-energy) ones $\Psi_<$. Let's choose some arbitrary nonzero high-energy cutoff Λ defining a shell of wave vectors around the Fermi surface. The electronic variables can then be written

$$\Psi_{\sigma, K} = \theta(|\xi_{\mathbf{k}}| - \Lambda)\Psi_{>, \sigma, K} + \theta(\Lambda - |\xi_{\mathbf{k}}|)\Psi_{<, \sigma, K}. \tag{2.6}$$

The slow modes are inside the shell $\pm \Lambda$ while the fast ones are outside, with $|\xi_{\mathbf{k}}|$, going up to the physical cutoff Λ_0, taken to be equal to the bandwidth, so that we are sure that the whole Brillouin zone is taken into account. Note that the cutoff is imposed only on momentum space, while the Matsubara frequencies remain unlimited. The LEEA $S_\Lambda\{\Psi_<\}$ is an action containing only slow modes, and gives the same partition function as S [Eq. (2.5)], or, formally,

$$Z = \int \mathcal{D}\bar{\Psi}_< \mathcal{D}\Psi_< e^{S_\Lambda\{\Psi_<\}}. \tag{2.7}$$

This means that $S_\Lambda\{\Psi_<\}$ is calculated by taking the *partial trace* over only fast modes in Eq. (2.4):

$$S_\Lambda\{\Psi_<\} = \ln \int \mathcal{D}\bar{\Psi}_> \mathcal{D}\Psi_> e^{S\{\Psi_<, \Psi_>\}}. \tag{2.8}$$

The LEEA contains an effective kinetic part $S_{0\Lambda}$ with a finite self-energy term and a new interaction $S_{I\Lambda}$. We have *chosen* that the Fermi surface for the bare electrons plays the role of the zero energy manifold. Certainly, this ceases to be the case if the form of the Fermi surface itself changes upon renormalization. If we however keep $\xi_{\mathbf{k}}$ for bookkeeping of mode elimination, both technical and conceptual difficulties can be encountered when Λ becomes close to the maximal

Fermi-surface shift. The cutoff than loses its physical meaning and becomes just a measure of how many electrons remain to be integrated. Ideally, the cure would be to renormalize around the floating (Λ-dependent) Fermi surface. Here we will develop the RG equations for a procedure using bare dispersion $\xi_{\mathbf{k}}$ for mode discrimination. This still does not mean the neglecting of the self-energy renormalization. We will formally derive the whole, exact flow equations.

If we consider the slow modes as parameters, expression (2.8) can be evaluated, at least formally, using the linked cluster theorem.[38] The result is composed of three terms:

$$S_\Lambda\{\Psi_<\} = S\{\Psi_<\} + \Omega_> + \delta S\{\Psi_<\}. \qquad (2.9)$$

Only the interaction part S_I of the action S can mix slow and fast modes,

$$S_I = S_I\{\Psi_<\} + S_I\{\Psi_>\} + S_I\{\Psi_<,\Psi_>\}, \qquad (2.10)$$

while S_0 is diagonal and can contain only one kind of mode in the same term:

$$S_0 = S_0\{\Psi_<\} + S_0\{\Psi_>\}. \qquad (2.11)$$

The first term in Eq. (2.9) is then only a constant from the point of view of the fast electrons, and is equal to $S_0\{\Psi_<\} + S_I\{\Psi_<\}$. $\Omega_>$ is the grand potential (times β) of the fast electrons as if they were decoupled from the slow ones:

$$\Omega_> = -\sum_{\mathbf{k}>} \ln(1 + e^{-\beta\xi_{\mathbf{k}}})$$

$$+ \sum \text{ (all connected clusters with } S_I\{\Psi_>\}).$$

$$(2.12)$$

This term gives only a shift of the total free energy of the system.

The term $\delta S\{\Psi_<\}$ in Eq. (2.9) is the most interesting one. It brings the corrections due to the scattering processes of the slow modes on the fast ones into the LEEA, and is given by the sum of all connected graphs composed of $S_I\{\Psi_>\} + S_I\{\Psi_<,\Psi_>\}$. If we draw the slow modes as external legs, the diagrams for $\delta S\{\Psi_<\}$ are the clusters with at least two legs. A few low-order diagrams for $\delta S\{\Psi_<\}$ are given in Fig. 1. The terms with two external legs, labeled by a, b, c, and d in Fig. 1, are the self-energy terms, renormalizing S_0. The terms with four legs e, f, g, and h renormalize the quartic interaction term S_I. The terms with six (i and j) and more legs are *created* by the mode elimination procedure.

Of physical interest is the LEEA for the electrons in the very vicinity of the Fermi surface ($\Lambda \ll E_F$). Even if the coupling is small, some of the loop diagrams will, at low temperature ($T < \Lambda$), attain large values depending on the form of the Fermi surface. For example, if the Fermi surface is not close to van Hove singularities the particle-particle (p-p) diagram (f in Fig. 1) for the four-point vertex with zero center of the mass momentum always has a logarithmic dependence like $\log(\Lambda_0/\Lambda)$, where Λ_0 is the initial cutoff equal to the bandwidth. If the Fermi surface is nested the particle-hole (p-h) diagram (e in Fig. 1) at $2\mathbf{k_F}$ behaves in the same way. In the Hubbard model close to half-filling the van Hove singularities make both loops squares of logarithms. The per-
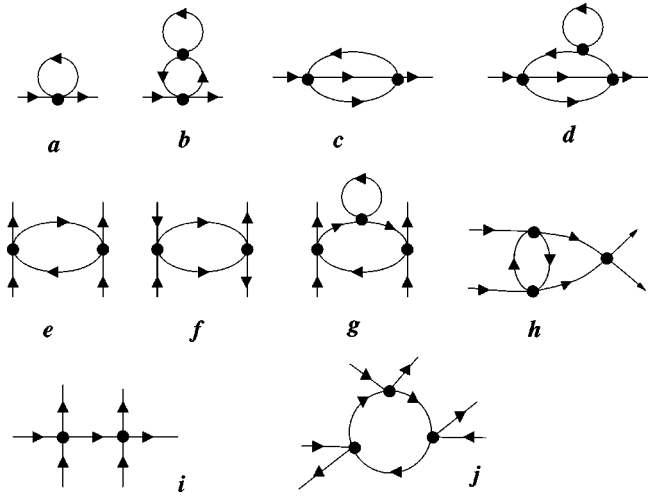
FIG. 1. A few lowest-order cumulants for $\delta S\{\Psi_<\}$. All internal lines are integrated only over the fast ($>$) modes.

turbative calculation of expansion (2.12) for small U_0 is thus not straightforward: at least some of sets of diagrams, containing *both p-p and p-h subdiagrams*, have to be summed entirely. The lowest order diagram of that kind is the one denoted by h in Fig. 1. On the other hand, the truncation of the LEEA at fourth order is in general allowed for weak coupling. However the direct summation of cumulants for $\delta S\{\Psi_<\}$ (like the T-matrix or RPA summation) can be performed in a useful and controlled way only for a limited number of physical problems, that is when some subsets of diagrams are dominant. The direct parquet summation for a general Fermi surface in more than one dimension is probably very hard. It was done only for the case of a perfectly nested (flat) Fermi surface.[20,21]

The problem is even more difficult if the coupling is not small. Then the criteria of most important sets of diagrams are no longer clear, and even the truncation of the LEEA at quartic or sextic term in $\Psi_<$ is no longer justified.

A. Kadanoff-Wilson-Polchinski renormalization group: Exact formulation

A tractable way to construct the *exact* LEEA is to use the Kadanoff-Wilson-Polchinski renormalization group. Let us call the initial cutoff (the bandwidth) Λ_0, and parametrize Λ by the renormalization parameter l so that $\Lambda = \Lambda_0 \exp(-l)$. The idea of the renormalization group is to consider the transformation $S \equiv S_{\Lambda_0} \to S'_{\Lambda_0 \exp(-l)}$ as an infinite set of infinitesimal mode eliminations

$$S_{\Lambda_0} \to S^{(1)}_{\Lambda_0 \exp(-dl)} \to S^{(2)}_{\Lambda_0 \exp(-2dl)} \to \cdots \to S'_{\Lambda_0 \exp(-l)}. \qquad (2.13)$$

At each step we eliminate Λdl of modes at a distance Λ from both sides of the Fermi surface. We will see that the mode elimination of an infinitesimal shell of degrees of freedom is much simpler than the one-step procedure discussed in Sec. I.

From now on we will simply call the LEEA the effective action because in the process of successive mode elimination [Eq. (2.13)] Λ can have any value between Λ_0 and zero. Indeed, it is of physical interest to follow the flow of the
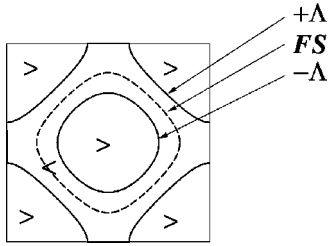
FIG. 2. The division of the Brillouin zone into the outer-shell ($>$), on-shell (l), and slow ($<$) modes.

effective action S_Λ as Λ decreases. We now concentrate to one single step $l \rightarrow l+dl$ of the mode elimination. We call *outer-shell* modes the modes already eliminated by the previous steps [the fast ($>$) modes]. The modes inside the shell [$\Lambda_0 \exp(-l) - \Lambda_0 \exp(-l-dl)$] are the ones to integrate out. We call them *on-shell* modes and denote them by (l). Figure 2 shows the division of the Brillouin zone into three types of modes ($>$, l, and $<$) for the case of the non-half-filled Hubbard model.

If l is not the very first step, the effective action S_Λ contains couplings of all orders. Schematically it reads

$$S_\Lambda = S_{0\Lambda} + S_{I\Lambda} = \Gamma_2^{(l)}\bar{\Psi}\Psi + \Gamma_4^{(l)}\bar{\Psi}\bar{\Psi}\Psi\Psi + \Gamma_6^{(l)}\bar{\Psi}\bar{\Psi}\bar{\Psi}\Psi\Psi\Psi$$
$$+\cdots. \qquad (2.14)$$

All Ψ's live only within the cutoff $\pm\Lambda$. The summation over all frequencies, momenta, and spins is assumed. The two-point vertex Γ_2 defines Wick's theorem at step l. In particular the propagator of the ''bare electrons'' Γ_2^{-1} changes as we proceed with the renormalization.

The construction of the effective action one step further (at $l+dl$) is of the same form as Eq. (2.9), with the difference that now the on-shell modes play the role of the fast modes. As we are interested only in the renormalization of vertices, we can skip the constant Ω, and we obtain the recursion relation

$$S_{\Lambda(l+dl)} = S_{\Lambda(l)} + \delta S(l). \qquad (2.15)$$

The contribution $\delta S(l)$ is due to the elimination of l modes. It is given by the sum of all cumulants made of $S_{I\Lambda}\{\Psi_l\}$ and $S_{I\Lambda}\{\Psi_l, \Psi_<\}$ with two or more legs, but now with all inter-
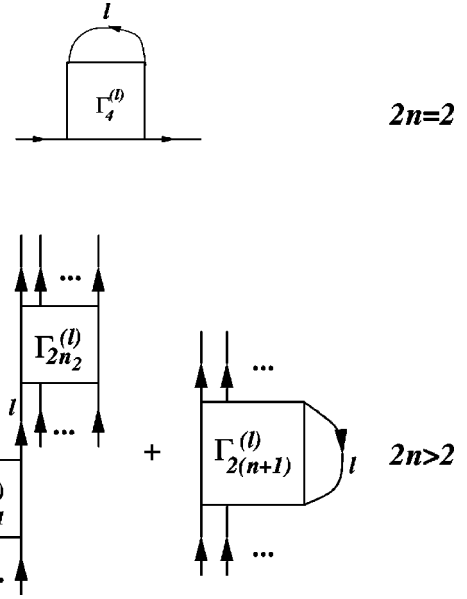
FIG. 3. Differential flow for the vertices with $n=2$ and $n>2$ legs. Lines ''l'' are dressed on-shell propagators.

nal momenta constrained to be on shell. Now we use the fact that $d\Lambda$ is infinitesimal: In the expression for $\delta S(l)$ only the terms linear in dl will survive, to make recursion (2.15) a differential equation for $S_{\Lambda(l)}$. Generally cumulants with m internal lines are proportional to $d\Lambda^m$, because every internal line is constrained to the shell. In principle only diagrams with one internal line are proportional to dl. If we group terms with equal number of legs, we obtain the flow equation for vertices $\Gamma_n^{(l)}$, known as the Polchinski equation for the vertices.[32,33] Only two types of diagrams with one internal line are possible: tree diagrams and loop diagrams. We obtain the recursion for the two-point vertex

$$\frac{\partial}{\partial\Lambda_l}\Gamma_2^{(l)}(K) = -T\sum_{\omega_n'}\int_{d\Lambda}d^2k'\,\Gamma_4^{(l)}(K',K,K',K)G_l(K').$$
$$(2.16)$$

This means that only the loop term renormalizes the self-energy (see Fig. 3). Both loop and tree terms are present in the recursion equation for the higher-order vertices:

$$\frac{\partial}{\partial\Lambda_l}\Gamma_{2n}^{(l)}(K_1,\ldots,K_n,K_{n+1},\ldots,K_{2n}) = \sum_{I_1,I_2}T\sum_{\omega_n}\int_{d\Lambda}d^2k\,\Gamma_{2n_1}^{(l)}(-K,I_1)G_l(K)\Gamma_{2n_2}^{(l)}(K,I_2)$$

$$-T\sum_{\omega_n}\int_{d\Lambda}d^2k\,\Gamma_{2(n+1)}^{(l)}(K,K_1,\ldots,K_n,K,K_{n+1},\ldots,K_{2n})G_l(K), \qquad (2.17)$$

also shown in Fig. 3. The two-point vertex defines the one-particle propagator G_l at each step of the renormalization:

$$G_l(K) = [\Gamma_2^{(l)}(K)]^{-1}. \qquad (2.18)$$

We use this *renormalized* propagator to construct the Wick theorem. Note that this is the difference between our ap-

proach and the standard Polchinski equation,[33] where all contractions are bare propagators. We call the vertex with $2n$ external legs at the step l of the renormalization, $\Gamma_{2n}^{(l)}(K_1,\ldots,K_n,K_{n+1},\ldots,K_{2n})$, with legs $\{K_1,\ldots,K_n\}$ coming in and $\{K_{n+1},\ldots,K_{2n}\}$ coming out. Symbols I_1 and I_2 in Eq. (2.17) are disjoint subsets ($I_1 \cap I_2 = \varnothing$) of the
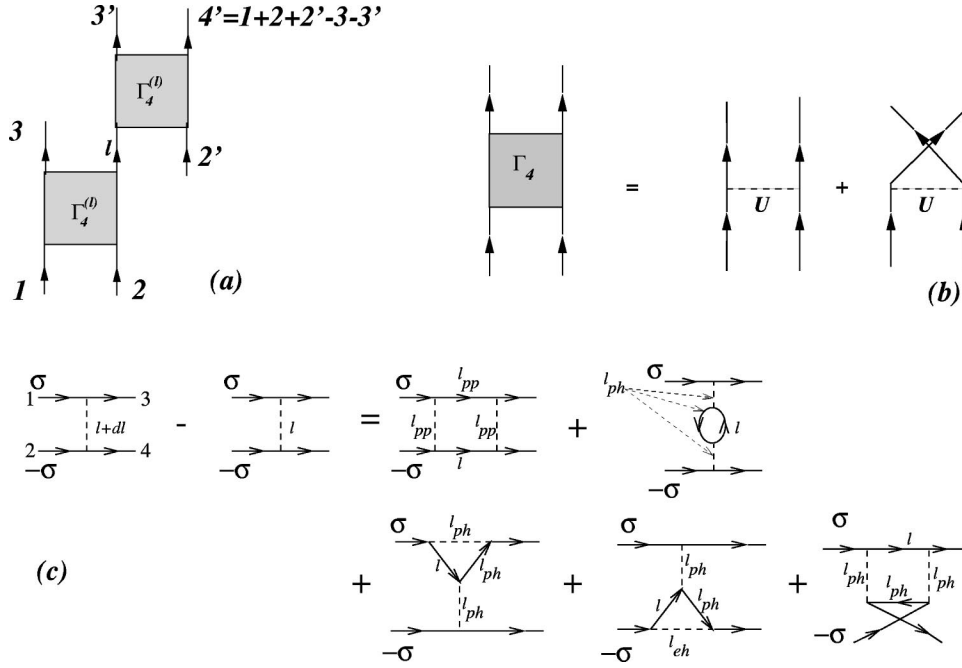
FIG. 4. (a) The six-point vertex for a one-loop renormalization group. (b) Relation between the vertex Γ_4 and the interaction U. (c) Recursion for the one-loop renormalization of the interaction U.

energies and momenta such that $I_1 \cup I_2 = \{K_1, \ldots, K_{2n}\}$. The sum runs over all such sets. We have skipped spin indices for simplicity.

We see that the Polchinski flow equation is a functional equation because all vertices are renormalized as *functions* of momenta and frequencies. It gives the exact renormalization-group flow of the model. In particular, this means that besides ''leading logarithmic'' contributions all other contributions are also taken into account. For example, if we are in two or more dimensions, and especially if the nesting is good but not perfect, the Polchinski equation takes correctly all ''almost logarithmic'' contributions into account.

In principle vertices of all orders are created with increasing powers of the initial coupling U_0: It is easy to see that the vertex Γ_{2n}, $(n>2)$, is created by the tree term of the Polchinski equation with power $(n-1)$ of the bare coupling. This means that the truncation of expansion (2.14) is equivalent to the weak-coupling perturbation theory.

B. Truncation of the Polchinski equation: one-loop renormalization group

The one-loop renormalization for the vertex Γ_4 (or for the effective interaction U_l) is the perturbative procedure to truncate the flow equations at order U^2. All terms of order higher than 6 in expansion (2.14) are created with a power higher than 2 of the interaction by the tree term of the Polchinski equation. Thus, putting $\Gamma_8 = \Gamma_{10} = \cdots = 0$, we generate the one-loop renormalization group. The only contribution to the vertex Γ_6 is then the tree term, made of two Γ_4 terms connected by one line [see Fig. 4(a)]. The line denoted by l has in principle to be taken dressed by the self-energy at the step l defined as

$$\Sigma_l \equiv \Gamma_2^{(l)} - \Gamma_2^0 = \Gamma_2^{(l)} - i\omega_n + \xi_{\mathbf{k}}. \qquad (2.19)$$

We assume that the self-energy remains diagonal upon renormalization. This is consistent with the weak-coupling treatment, because off-diagonal terms would imply the existence of some form of long-range order, which is out of the reach of the present calculation. All we can possibly expect from our calculation is a divergence of some effective interaction signaling the *onset* of a long-range order in a mean-field sense.

We now go back to the formulation in terms of the interaction as defined by Eq. (2.5) and illustrated in Fig. 4(b). We will skip the spin indices where they are not necessary. The differential flow of the six-point function Γ_6 at step l is according to Fig. 4(a) given by

$$d\Gamma_6^{(l)}(K_1, K_2, K_3, K_2', K_3')$$

$$= T\sum_{\omega_n} \int_{d\Lambda} d^2k \; \delta(\mathbf{k} - \mathbf{k}_1 - \mathbf{k}_2 + \mathbf{k}_3) \, \delta_{\omega_n - \omega_{n1} - \omega_{n2} + \omega_{n3}}$$

$$\times G_l(K) U_l(K_1, K_2, K_3) U_l(K, K_2', K_3'). \qquad (2.20)$$

The phase-space integral is over the shell of thickness $d\Lambda$ corresponding to step l, and $G_l(K)$ is the renormalized Green function at the same step. Physically this is the propagator of an on-shell electron renormalized by the scattering on the fast electrons. $U_l(K_1, K_2, K_3)$ is the effective interaction at step l. The vertex Γ_6 at some step l is the integral of Eq. (2.20) over all steps between $\Lambda = \Lambda_0$ and Λ_l, that is, over all fast degrees of freedom. On the other hand, there is no loop integration in this term: the Dirac function in Eq. (2.20) reduces the integral $\int_{d\Lambda} d^2k$ to a single point $\mathbf{k} = \mathbf{k}_1 + \mathbf{k}_2 - \mathbf{k}_3$ $(= \mathbf{k}_{3'} + \mathbf{k}_{4'} - \mathbf{k}_{2'})$. To obtain Γ_6 we can thus skip the integration over dl and take care of the momentum conservation. The effective action at the step l then reads

$$S_l = \sum_{\omega_n, \mathbf{k}} \bar{\Psi}_{K,\sigma} [i\omega_n - \xi_{\mathbf{k}} + \Sigma_l(K)] \Psi_{K,\sigma} \Theta[\Lambda(l) - |\xi_{\mathbf{k}}|]$$

$$+ \frac{1}{2} T^3 \sum_{\sigma\sigma'} \sum_{1,2,3} U_l(K_1, K_2, K_3)$$

$$\times \Theta^{(\Lambda(l))}_{\mathbf{k}_1, \mathbf{k}_2, \mathbf{k}_3, \mathbf{k}_4} \bar{\Psi}_{\sigma K_3} \bar{\Psi}_{\sigma' K_4} \Psi_{\sigma' K_2} \Psi_{\sigma K_1}$$

$$+ T^5 \sum_{\sigma, \sigma', \sigma''} \sum_{1,2,3,2',3'} [\Theta^{(\Lambda(l))}_{\mathbf{k}_1, \mathbf{k}_2, \mathbf{k}_3, \mathbf{k}_2', \mathbf{k}_3', \mathbf{k}_4'}$$

$$\times \Theta[|\xi_{\mathbf{k}}| - \Lambda(l)] G_{l'}(K) U_{l'}(K_1, K_2, K_3)$$

$$\times U_{l'}(K, K_2', K_3') \bar{\Psi}_{\sigma K_3} \bar{\Psi}_{\sigma' K_3'} \bar{\Psi}_{\sigma'' K_4'}$$

$$\times \Psi_{\sigma'' K_2'} \Psi_{\sigma' K_2} \Psi_{\sigma K_1}], \qquad (2.21)$$

where $l' = \ln \Lambda_0/|\xi_{\mathbf{k}}|$ [i.e., $\xi_{\mathbf{k}} = \Lambda(l')$] is the scale fixed by external momenta, $K = K_1 + K_2 - K_3$ and the energy-momentum vector $4' = 1 + 2 + 2' - 3 - 3'$. The summations over $1,2,3,\dots$ run over corresponding Matsubara frequencies and momenta. The term of the sixth-order contains the interactions and Green functions from former steps $l' < l$ of the mode elimination since only fast degrees of freedom contribute to Γ_6^l so that $l' \le l$. This constraint is imposed to the sextic term of action (2.21) by $\Theta[|\xi_{\mathbf{k}}| - \Lambda(l)]$. The functions $\Theta^{(\Lambda)}_{\mathbf{k}_1, \mathbf{k}_2, \mathbf{k}_3, \mathbf{k}_4}$ and $\Theta^{(\Lambda)}_{\mathbf{k}_1, \mathbf{k}_2, \mathbf{k}_3, \mathbf{k}_2', \mathbf{k}_3', \mathbf{k}_4'}$ constrain the momenta in arguments to be slow modes (inside a shell of thickness $\pm\Lambda$ around the Fermi surface). This simply means that the fields described by the effective action at cutoff $\Lambda(l)$ are inside the cutoff range.

If the initial interaction U_0 is spin independent, the renormalized interaction U_l will remain spin independent as well. It is thus not necessary to worry about spin indices and all two-particle interactions are given only by *one* function $U_l(1,2,3)$. The detailed justification for this is given in the Appendix. The differential flow of $U_l(1,2,3)$ is readily obtained by applying the loop term of the Polchinski equation [the second term in Eq. (2.17) and in Fig. 3(b)] to the six-leg part of the effective action (2.21). At first sight, two kinds of diagrams are created: a one–particle reducible (1PR) diagram and a one-particle irreducible (1PI) diagram. We will show that only 1PI diagrams contribute to the renormalization of the effective interaction: We can try to construct the 1PR diagram by contracting legs $2'$ and $4'$ in Fig. 4(a). This immediately implies that the internal line denoted with l and the leg $3'$ carry the same momentum. This momentum corresponds to some fast mode since line l is already integrated out. The conclusion is that the resulting four-point 1PR vertex cannot be a vertex of the effective action (2.21), since this action contains only slow modes. Consequently, only 1PI diagrams renormalize the effective interaction between slow electrons. The resulting diagrams are all topologically different two-particle loops as shown in Fig. 4(c). The first diagram is a p-p diagram, and the others are p-h diagrams. Let us illustrate how we obtain the first diagram in Fig. 4(c). The procedure is shown in Fig. 5. The diagram represents the p-p contribution to the effective interaction $U_l(1,2,3)$ due to the elimination of the infinitesimal shell at step l. We take the six-leg diagram with the configuration of external mo-
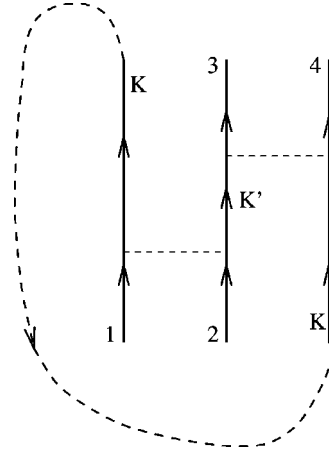
FIG. 5. Construction of the p-p diagram from the six-leg vertex.

menta shown in the figure, with legs K being on shell. Their contraction (dashed line) is done precisely at step l. The contraction K' was done at a previous step l_{pp} fixed by momenta K, K_1, and K_2 [see Eq. (2.20)]. $K_1 + K_2 = Q_{pp} \equiv (\omega_{npp}, \mathbf{q}_{pp})$ is the total energy-momentum vector in the p-p process. The scale l_{pp} is then given by

$$l_{pp} = -\ln \frac{|\xi_{\mathbf{k}-\mathbf{q}_{pp}}|}{\Lambda_0}. \qquad (2.22)$$

Similar constructions give all other $(p$-$h)$ diagrams. One has to take care of both direct and exchange interactions [Fig. 4(b)] to obtain four different graphs. The interactions and one-particle propagators are to be taken at the scale $l_{ph} \le l$. This scale is determined by the momentum transfer $\mathbf{q}_{ph}$ as

$$l_{ph} = -\ln \frac{|\xi_{\mathbf{k}+\mathbf{q}_{ph}}|}{\Lambda_0}. \qquad (2.23)$$

In the second, third, and fourth diagrams in Fig. 4(c), the energy-momentum transfer is $Q_{ph} = K_1 - K_3$, while in the last diagram $Q_{ph} = K_1 - K_4$.

We see that even though the Polchinski equation appears to be local in l, the flow at step l depends on the Green functions and interactions at the former steps $l_{pp}, l_{ph} \le l$. The reason for this is the dependence of the six-point function on the two-particle interaction, and on the one-particle propagator at all former steps.

In Fig. 4(c) the internal lines labeled l are to be integrated over two infinitesimal shells of the width $d\Lambda$ at $\xi_0 = \pm\Lambda_l$. For this purpose we pass from the Cartesian measure $dk_x dk_y$ to the measure

$$\int_{\xi}^{\xi+d\Lambda} d\xi' \oint \frac{ds}{v(s,\xi')}, \qquad (2.24)$$

where s are lines (or surfaces in $D > 2$) of constant energy $\xi(\mathbf{k})$ and $v(s,\xi')$ is the group velocity as defined by $\partial\xi(\mathbf{k})/\partial k_\perp$ ($k_\perp$ is the component of the momentum perpendicular to the equal-energy lines). We will use measure (2.24) in what follows, where we write the analytic expression for the flow of function $U_l(1,2,3)$.

From the diagrams in Fig. 4(c) one obtains the expression

$$\frac{\partial U_l}{\partial l} = \beta(l,\{U\}) = \beta_{pp}\{U,U\} + 2\beta_{ph}\{U,U\} - \beta_{ph}\{U,XU\}$$

$$- \beta_{ph}\{XU,U\} - X\beta_{ph}\{XU,XU\}. \tag{2.25}$$

β is a four-point object and a bilinear functional of $U_{l'}$, $(l' \leq l)$. The operator X is the exchange operator acting on a four-point function: $XF(1,2,3,4) \equiv F(2,1,3,4)$. β_{pp} and β_{ph} are the p-p and p-h parts of the β function given by

$$\beta_{pp}\{U,U\} = \Xi\{U,U\} + \Xi\{XU,XU\}, \tag{2.26}$$

$$\beta_{ph}\{U_1,U_2\} = \Pi\{U_1,U_2\} + \mathcal{T}\Pi\{U_1,U_2\}. \tag{2.27}$$

$\mathcal{T}$ is the time inversion operator acting on a four-point function: $\mathcal{T}F(1,2,3,4) \equiv F(3,4,1,2)$. The functions Ξ and Π correspond to the on-shell integrals of the p-p and p-h bubbles:

$$\Xi\{U,U\}(K_1,K_2,K_3,K_4)$$

$$= \frac{-\Lambda_l}{(2\pi)^2} \sum_{\nu=+,-} \int \frac{ds_\nu}{v_\nu} \Theta(|\xi_{\mathbf{k}_\nu - \mathbf{q}_{pp}}| - \Lambda_l)T$$

$$\times \sum_{\omega_n} G_l(K_{(\nu)}) G_{l_{pp}}(-K_{(\nu)} + Q_{pp})$$

$$\times U_{l_{pp}}(K_1,K_2,K_{(\nu)}) U_{l_{pp}}(K_3,K_4,K_{(\nu)}), \tag{2.28}$$

$$\Pi\{U_1,U_2\}(K_1,K_2,K_3,K_4)$$

$$= \frac{-\Lambda_l}{(2\pi)^2} \sum_{\nu=+,-} \int \frac{ds_\nu}{v_\nu} \Theta(|\xi_{\mathbf{k}_\nu + \mathbf{q}_{ph}}| - \Lambda_l)T$$

$$\times \sum_{\omega_n} G_l(K_{(\nu)}) G_{l_{ph}}(K_{(\nu)} - Q_{ph})$$

$$\times U_{1,l_{ph}}(K_1,K_{(\nu)},K_3) U_{2,l_{ph}}(K_4,K_{(\nu)},K_2). \tag{2.29}$$

U_1 and U_2 can be U or XU as required by Eq. (2.25). The summation over index $\nu = +,-$ is over two shells at $\xi_0 = \pm\Lambda_l$; the velocities are $v_\nu = v(s_\nu, \xi = \nu\Lambda)$, and K_ν symbolizes $(\mathbf{k}_\nu, \omega_n)$. The quantity

$$Q_{pp} = (\omega_{n,pp}, \mathbf{q}_{pp}) = K_1 + K_2$$

is the total energy-momentum vector, and

$$Q_{ph} = (\omega_{n,ph}, \mathbf{q}_{ph}) = K_1 - K_3,$$

is the energy-momentum transfer between the currents $(1,3)$ and $(2,4)$ where 1, 2, 3, and 4 are the external variables of Ξ and Π. The scales l_{pp} and l_{ph} are defined by expressions (2.22) and (2.23). As already discussed, l_{pp} and l_{ph} depend on the integration variable $\mathbf{k}_\nu$ and on the configuration of the external energy momenta. Let us call the external legs of the total β function [Eq. (2.25)] $\tilde{1}$, $\tilde{2}$, $\tilde{3}$, and $\tilde{4}$. Note that the operator X exchanges the external legs $\tilde{1}$ and $\tilde{2}$ in the last term of this expression. This means that the energy-momentum transfer in this term is $Q_{ph} = K_{\tilde{1}} - K_{\tilde{4}}$ and not $K_{\tilde{1}} - K_{\tilde{3}}$, as in the first three e-h terms. In the standard language (see, for example, Ref. 31), the p-h terms with transfers 1–3 are called zero-sound (ZS) terms, and the terms with transfers 1–4 are ZS$'$.

Let us explain briefly how we obtained the flow equation (2.25). The first term is simply the p-p loop with U interaction. The remaining terms are different versions of the p-h loops, corresponding respectively to the p-h diagrams in Fig. 4(c). They can all be seen as a single loop β_{ph} [with the topology of the second diagram in Fig. 4(c)], given by Eqs. (2.27) and (2.29) by performing appropriately the operation X. The third and fourth graphs can be drawn as the second one-by-one exchange: In the third term we replace the upper interaction line U by XU, and in the fourth we replace the lower one. After this manipulation both diagrams look like the second diagram. The last graph is more complicated: one has to perform X upon both interactions and upon the whole graph to see it as β_{ph}. The factor 2 before the second term is due to spin summation in the loop. All other diagrams have a fixed spin.

The flow of the effective action (2.21) is still not completely determined because we do not know how the self-energy $\Sigma_l(K)$ is renormalized. The differential flow for $\Sigma_l(K)$ is readily found from the Polchinski equation for the two-point function (2.16) shown graphically in Fig. 3. In the language of the effective interaction $U_l(1,2,3)$ this gives Hartree-Fock-like contributions shown in Fig. 4(c). We obtain the renormalization equation

$$\frac{\partial\Sigma(K_1)}{\partial l} = \alpha_{\text{Hartree}}\{U_l\}(K_1) + \alpha_{\text{Fock}}\{U_l\}(K_1) + \alpha_\mu^{\text{hom.}}(l). \tag{2.30}$$

The first term is the Hartree term

$$\alpha_{\text{Hartree}}\{U_l\}(K_1) = \frac{\Lambda}{(2\pi)^2} \sum_{\nu=+,-} \int \frac{ds_\nu}{v_\nu} T \sum_{\omega_n} G_l(K_\nu)$$

$$\times \frac{1}{2}(3-X)U_l(K_1,K_\nu,K_1), \tag{2.31}$$

and the second is the exchange term

$$\alpha_{\text{Fock}}\{U_l\}(K_1) = -\frac{\Lambda}{(2\pi)^2} \sum_{\nu=+,-} \int \frac{ds_\nu}{v_\nu} T \sum_{\omega_n} G_l(K_\nu)$$

$$\times \frac{1}{2}(1-X)U_l(K_\nu,K_1,K_1). \tag{2.32}$$

The third term is added to cancel the chemical potential renormalization due to the homogeneous part of the direct term

$$\alpha_\mu^{\text{hom.}}(l) = -\frac{1}{(2\pi)^2} \int d^2k_1 T \sum_{\omega_{n1}} \alpha_{\text{Hartree}}\{U_l\}(K_1). \tag{2.33}$$

If the initial interaction has no dynamics, the first nontrivial contributions to the flow of the self-energy come from the *renormalized* interaction and not the bare interaction. As the interaction is renormalized by one-loop processes this implies that the interesting part of the flow of $\Sigma_l(K)$ is given by two loops. On the level of the present one-loop calculation it is thus consistent to neglect self-energy corrections. This is what we do in the subsequent one-loop renormalization of the Hubbard model.
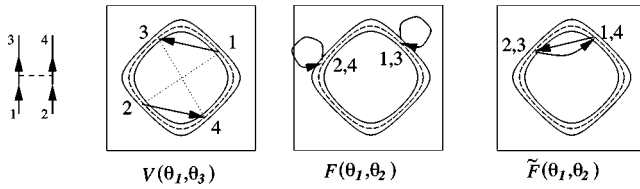
FIG. 6. The marginal interactions in the BCS regime.

III. RENORMALIZATION GROUP FOR THE HUBBARD MODEL

In this section we will apply the above renormalization-group procedure to the Hubbard model. The model is given by Eqs. (2.1), (2.2), and (2.3). The initial action S for the Hubbard model is given by expression (2.5), with the dispersion (2.3) and with the initial interaction $U_0 = \text{const}(K_1, K_2, K_3)$. The interaction will depend more and more on (K_1, K_2, K_3) as we go on with the renormalization (as l increases), so that we will see the functional aspect of our renormalization group at work. We will complete our analysis by the renormalization of two-particle correlation functions.

A. Renormalization of the interaction

If we neglect the self-energy corrections, the flow of the effective interaction is completely determined by expressions (2.25)–(2.29) with the bare propagators instead of the renormalized ones:

$$G_l(K) \rightarrow G_0(K) \equiv (i\omega_n - \xi_{\mathbf{k}})^{-1}. \qquad (3.1)$$

The effective interaction is a function of three energy-momenta vectors. This makes formulas (2.28) and (2.29) very complicated. For that reason we will consider only the marginal part of the dependence of U_l on energies and momenta. This approximation is justified by the zero-order scaling and power-counting arguments.[23,24,31] For example, in one dimension this procedure justifies the well-known g-ology model:[15] one adds an index i to the electrons so that all electrons moving to the left have $i = -$, and all right movers have $i = +$. Then the marginal interactions do not depend on impulse k and energy ω of the electrons in interaction, but only on their indices i. This can be seen as parametrization of the interactions as if the electrons were on the Fermi surface (or points in one dimension) with $\omega = 0$. In two dimensions the marginal interactions depend only on polar coordinates of the wave vectors. Only the interactions between electrons at the Fermi surface are then kept and, if the Fermi surface is not nested, one obtains the LEEA for the Fermi liquid.[24,31] The marginal processes in that case are

$$V(\theta_1, \theta_2) = U_l(K_1, -K_1, K_2), \quad \omega_{1,2} = 0, \quad \xi_{\mathbf{k}_{1,2}} = 0 \qquad (3.2)$$

and

$$F(\theta_1, \theta_2) = U_l(K_1, K_2, K_1), \quad \omega_{1,2} = 0, \quad \xi_{\mathbf{k}_{1,2}} = 0,$$

$$\tilde{F}(\theta_1, \theta_2) = X U_l(K_1, K_2, K_1) = U_l(K_1, K_2, K_2),$$

$$\omega_{1,2} = 0, \quad \xi_{\mathbf{k}_{1,2}} = 0. \qquad (3.3)$$
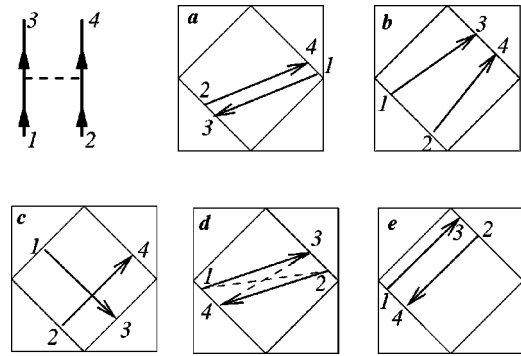
FIG. 7. Some of the marginal processes for the square Fermi surface.

V is the pairing amplitude, while F and $\tilde{F}$ are the forward and the backward scattering related to the Fermi-liquid parameters. The three kinds of processes are shown in Fig. 6 for the case of a Hubbard model far from half-filling. We analyzed this problem in detail in a previous paper.[23]

Let us now concentrate on the square Fermi surface, for the half-filled Hubbard model. The processes between electrons on the Fermi surface are now labeled with three variables instead of two, as in the case of the Fermi surface without nesting: if we put particles 1, 2, and 3 *anywhere* on one side or on two opposite sides of the square, the fourth falls exactly on the square as well. This is due to the perfect flatness of the Fermi surface and to the marginality of the umklapp processes. A few examples of marginal interactions between the electrons on the square are shown in Fig. 7. The interaction depends only on the positions of the particles on the square. The "angle" θ can be defined in a way shown in our previous paper.[37] It is important to notice that even if the filling is not exactly one-half (and the Fermi surface not exactly square), all above interactions will still be important, as long as the effective phase space is open, i.e., when $\Lambda > |\mu|$. We thus take as marginal all effective interactions viewed as functions of three angles θ of the particles:

$$U_l(K_1, K_2, K_3) \rightarrow U_l(\theta_1, \theta_2, \theta_3),$$

$$\omega_{1,2,3,4} = 0, \quad 1,2,3,4 \text{ are on the square.} \qquad (3.4)$$

When the cutoff becomes smaller than the chemical potential, we are back to the nonnested case, in which the functions V and F are the marginal interactions. They read

$$V_l(\theta_1, \theta_2) = U_l(\theta_1, \theta_1 + \pi, \theta_2),$$

$$F_l(\theta_1, \theta_2) = U_l(\theta_1, \theta_2, \theta_1). \qquad (3.5)$$

Altogether, for the half- and almost half-filled Hubbard models the function $U_l(\theta_1, \theta_2, \theta_3)$ given by Eq. (3.4) contains all marginal scattering processes. The renormalization-group analysis is now much simpler because we deal with a function of three variables instead of nine.

We will now derive the flow equation for $U_l(\theta_1, \theta_2, \theta_3)$ at zero temperature. After replacing $G_l(K)$ by $G_0(K)$ and $U_l(K_1, K_2, K_3)$ by $U_l(\theta_1, \theta_2, \theta_3)$ in expressions (2.28) and (2.29), we can perform the Matsubara summations analytically. After taking the $T \rightarrow 0$ limit we obtain

$$\Xi\{U,U\}(\theta_1,\theta_2,\theta_3) = \frac{-2}{(2\pi)^2} \sum_{\nu=+,-} \int d\theta \mathcal{J}(\nu\Lambda,\theta)$$

$$\times \frac{\Theta(\nu\xi_{\mathbf{k}_\nu-\mathbf{q}_{pp}})\Theta(|\xi_{\mathbf{k}_\nu-\mathbf{q}_{pp}}|-\Lambda)}{1+\frac{\nu}{\Lambda}\xi_{\mathbf{k}_\nu-\mathbf{q}_{pp}}}$$

$$\times U_{l_{pp}}(\theta_1,\theta_2,\theta)U_{l_{pp}}(\theta_3,\theta_4,\theta),$$

$$(3.6)$$

$$\Pi\{U_1,U_2\}(\theta_1,\theta_2,\theta_3)$$

$$= \frac{2}{(2\pi)^2} \sum_{\nu=+,-} \int d\theta \mathcal{J}(\nu\Lambda,\theta)$$

$$\times \frac{\Theta(-\nu\xi_{\mathbf{k}_\nu+\mathbf{q}_{ph}})\Theta(|\xi_{\mathbf{k}_\nu+\mathbf{q}_{ph}}|-\Lambda)}{1-\frac{\nu}{\Lambda}\xi_{\mathbf{k}_\nu+\mathbf{q}_{ph}}}$$

$$\times U_{1,l_{ph}}(\theta_1,\theta,\theta_3)U_{2,l_{ph}}(\theta_4,\theta,\theta_2). \quad (3.7)$$

$\mathbf{k}_\nu$ is the momentum of a particle at the angle θ with energy $\xi=\nu\Lambda$. $\mathcal{J}(\epsilon,\theta)\equiv J[(x,y)/(\epsilon,\theta)]=(\partial s/\partial\theta)/v(\theta,\epsilon)$ is the Jacobian of the transformation from rectangular coordinates in momentum space to polar coordinates. One should not forget that the scales l_{pp} and l_{ph}, which make the flow equation nonlocal, depend on external momenta and on the integration variable θ through $\mathbf{q}_{pp}$, $\mathbf{q}_{ph}$, and $\mathbf{k}_\nu$, as given by relations (2.22) and (2.23). U_1 and U_2 represent U or XU as required by Eq. (2.25). Equation (3.6) gives the leading logarithmic flow in the p-p channel for the configuration of momenta with $\mathbf{q}_{pp}=0$, while Eq. (3.7) gives the leading logarithmic flow in the p-h channel only exactly at half-filling for $\mathbf{q}_{ph}=(\pi,\pi)$. In the standard renormalization-group procedure,[31] only configurations of these kinds are renormalized. We see that in our formalism they are taken into account on an equal footing with all other scattering processes, with any values of $\mathbf{q}_{pp}$ and $\mathbf{q}_{ph}$, as illustrated in Fig. 7. The processes with the leading logarithmic renormalization in one channel and with less strong but still important flow in the other channel [like the processes in Figs. 7(d) and 7(e)] are the processes which strongly couple both renormalization channels. For example, the process in Fig. 7(d) has leading logarithmic renormalization in the p-p channel, and a less strong (but still logarithmic, because of partial nesting) renormalization in the p-h channel, while the process in Fig. 7(e) has perfect nesting and, consequently, a greater logarithmic flow in the p-h channel and a weaker logarithmic flow in the p-p channel.

The advantage of the Kadanoff-Wilson-Polchinski mode elimination technique at $T=0$ upon renormalization schemas based on field theory renormalization[23] is that in the KWP approach Λ can be interpreted as the temperature. That is, the interaction at some temperature T is renormalized mainly by virtual processes involving ''quantum'' electrons, those with energy larger than T, having almost the same distribution as the $T=0$ electrons. This is exactly what we do with the renormalization group: only modes with $|\xi_{\mathbf{k}}|>\Lambda$ are involved in the virtual processes renormalizing U_l. Conse-

quently, Λ is not only the measure of how many electrons are already integrated out: it has a *physical* meaning of the effective temperature. Given that effective ''microscopic'' degrees of freedom live inside the cutoff range, this cutoff also plays the role of the best energy resolution one can obtain for correlation functions at a given step of renormalization. In fact, all features with characteristic energies lower than Λ are smeared. All these nice aspects are in general not present in the field-theory approach, whose only advantage is that the RG equation are local in Λ. There, if we want to obtain the correct temperature (or energy) dependence of the vertex, we have to integrate the whole flow down to $\Lambda=0$, with temperature T taken as the input parameter.

Let us concentrate briefly on the nonlocality of our equations, which is a consequence of the KWP scheme. On can also ask why we do not use the 1PI scheme,[33] which is local and apparently simpler. The answer is related to the fact that both Polchinski and 1PI versions are written for vertices with *full* energy-momenta dependences. In that sense, if we were able to keep all (K_1, K_2, and K_3) dependences of the vertex, the 1PI version would indeed be simpler. But the very point of our calculations is that we neglect all energy dependences (radial momenta and frequencies) of the vertex, except the one on Λ. If we apply this approximation to the Polchinski equation, in a correct way we still keep (in the RG sense) the dependence of the vertex on outer-shell momenta. That is, the assumption that U has only an angular dependence is made for slow modes only. This is implicit in our approach because the Wilsonian action with a hard cutoff contains only slow modes, so that the legs of U can be only within the cutoff range. On the other hand, we can also formally explore the Polchinski-like flow of a particular four-point vertex with one fast leg (with energy $\xi>\Lambda$) and three slow legs. At least on the one-loop level, it can be shown[41] that this vertex can be replaced by the same vertex at former $\Lambda'=\xi$. There all energies can be set to zero, including ξ, in the spirit of our approximation of only angular dependence. This vertex is the one intervening in our nonlocal RG equations. We just say that it can be replaced by another vertex, at actual cutoff, but with an outer-shell dependence on ξ taken into account. This means that if we want our RG to be local in Λ, we have to pay it by supplementary energy dependence. If we ignore both nonlocality and the ξ dependence, the flow is overestimated. On the other hand, the 1PI procedure gives local equations for all vertices. We can try to apply our approximation of ''no energy dependence'' directly to this, just as we did to the vertices of Wilsonian effective action. The same reasoning as above brings us to the conclusion that for all vertices with at least one fast leg at least one energy scale should be kept other than the cutoff itself. Thus the 1PI scheme, once carefully applied, becomes just as complicated as the KWP scheme.

If we want to see which series of diagrams is generated by our renormalization group, we have to solve the differential equation (2.25) for U_l in iterations of the bare interaction U_0. The obtained series is exactly the parquet summation. It is constructed from all iterations of five basic loop diagrams from Fig. 4(c). A few lowest-order parquet diagrams are shown in Fig. 8.

An important aspect of the non-half-filled Hubbard model is that it cannot be solved by a scale-invariant renormaliza-
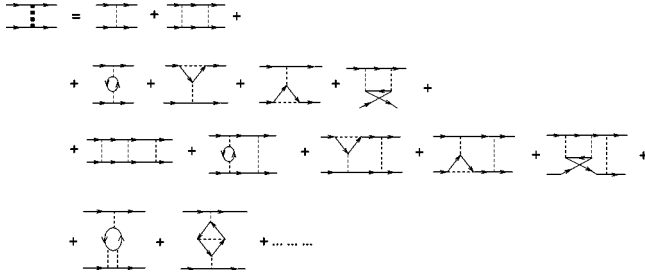
FIG. 8. The parquet summation.

tion group. The finite chemical potential determines the intrinsic scale, the physical interpretation of which is the crossover between two different renormalization regimes. The crossover can be seen from the *explicit* scale dependence of p-p and p-h differential loops $\Xi(l)$ and $\Pi(l)$. We can define the quantities

$$\beta_{pp}^0(l) = \Xi_l\{1,1\}_{\mathbf{q}_{pp}=0}, \qquad (3.8)$$

$$\beta_{ph}^0(l) = \Pi_l\{1,1\}_{\mathbf{q}_{ph}=(\pi,\pi)}. \qquad (3.9)$$

They measure the dominant parts of the p-p and p-h renormalization tendencies, respectively. The configurations of momenta are chosen to give the most important flow: for the p-p channel at zero total momentum and for the p-h channel at the antiferromagnetic wave vector. The quantities $\beta_{pp}^0(l)$ and $\beta_{ph}^0(l)$ are shown in the Fig. 9 for a finite chemical potential $\mu = -\Lambda_0 \exp(-l_\mu)$.

We see that for $l < l_\mu$ both differential loops have linear dependences on the logarithmic variable l; the total (integrated) loops are thus square logarithmic, as is known for the half-filled band. When $l > l_\mu$ the function $\beta_{pp}^0(l)$ crosses over to constant, which gives the logarithm of the Cooper bubble. $\beta_{ph}^0(l)$ decays exponentially as $\exp(-2l) \sim \Lambda^2$: the nesting no longer exists, and the p-h flow crosses over to irrelevance. We call the first regime the parquet regime because both loops are important. The second regime, in which only the Cooper channel flows, we call the BCS regime. The
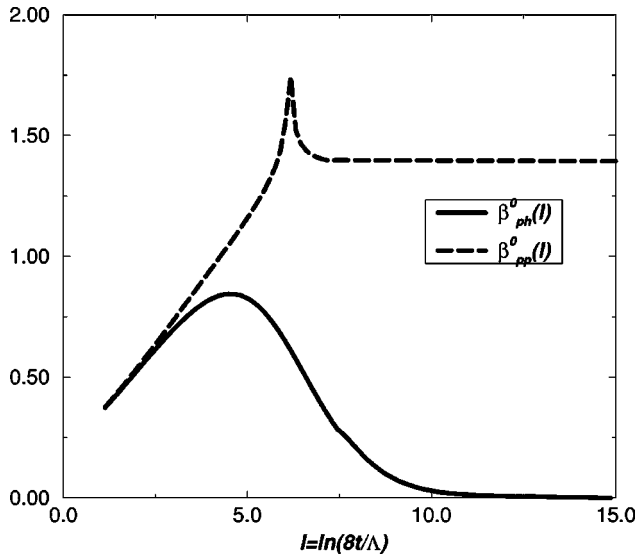
FIG. 9. The quantities $\beta_{pp}^0(l)$ and $\beta_{ph}^0(l)$. The crossover is at $l = l_\mu = 6$.
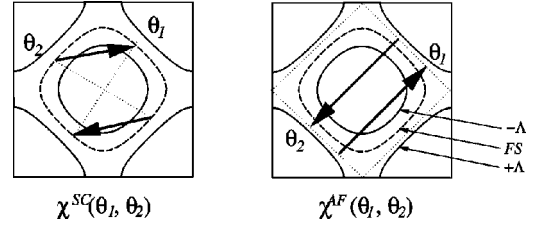
FIG. 10. The angle-dependent correlation functions.

topology of the effective phase space in the parquet regime is open (see Fig. 2), and in the BCS regime the phase space is a regular closed ring around the Fermi surface, as in Fig. 6. The peak of $\beta_{pp}^0(l)$ at $l = l_\mu$ is the enhancement due to van Hove singularity. The peak does not exist in $\beta_{ph}^0(l)$ because of the Θ-function constraint in Eq. (3.7). As we will see below, the renormalization in the parquet regime will give rise to precursors of a strong-coupling fixed point with dominant antiferromagnetic correlations, while in the BCS regime only a Cooper-like instability is possible.

It is difficult to see from the sole flow of the interaction U_l what kind of correlations are enhanced and possibly divergent. For that purpose we have to calculate the renormalization of the correlation functions.

B. Renormalization of the correlation functions

It is well known[23,24,31,40] that, in studying the anisotropic superconductivity, one has to consider the pairing amplitude as a function of two angles, $V(\theta_1, \theta_2)$. The angles determine the angular positions of the Cooper pairs annihilated (θ_1) and created (θ_2) in the scattering. This interaction will be intimately related to the superconducting correlation function $\chi^{SC}(\theta_1, \theta_2)$. In the same spirit we can define the correlation function for the antiferromagnetism dependent on two angles. We will define both correlation functions as

$$\chi_{\mathbf{q}}^{\delta}(\theta_1, \theta_2; |\tau_1 - \tau_2|) = \int_{>} d\epsilon_1 \int_{>} d\epsilon_2 \mathcal{J}(\epsilon_1, \theta_1) \mathcal{J}(\epsilon_2, \theta_2)$$

$$\times \langle \hat{\Delta}_{\mathbf{q}}^{\delta}(\epsilon_1, \theta_1; \tau_1) \tilde{\hat{\Delta}}_{\mathbf{q}}^{\delta}(\epsilon_2, \theta_2; \tau_2) \rangle,$$

$$(3.10)$$

with δ equal to SC or AF. The symbols ">" mean that the energy integrations run over energies *outside* of the shell $\pm \Lambda$. Consequently, χ^{SC} and χ^{AF} are interpreted as the susceptibilities at the temperature $T = \Lambda$. They measure the response of outer shell electrons for given Λ. The order parameter variables are

$$\hat{\Delta}_{\mathbf{q}}^{SC}(\epsilon, \theta; \tau) \equiv \sum_{\sigma} \sigma \Psi_{\sigma, \mathbf{k}}(\tau) \Psi_{-\sigma, -\mathbf{k}+\mathbf{q}}(\tau), \quad (3.11)$$

$$\hat{\Delta}_{\mathbf{q}}^{AF}(\epsilon, \theta; \tau) \equiv \sum_{\sigma} \bar{\Psi}_{\sigma, \mathbf{k}}(\tau) \Psi_{-\sigma, \mathbf{k}+(\pi,\pi)+\mathbf{q}}(\tau), \quad (3.12)$$

where $\mathbf{k}$ is given by the angle θ and the energy ϵ. Note that $\hat{\Delta}_{\mathbf{q}}^{SC}$ is a singlet. To obtain a triplet, one just skips the factor σ in the sumation over σ. Figure 10 illustrates what configurations of four angles are described by the correlation functions $\chi^{SC}(\theta_1, \theta_2)$ and $\chi^{AF}(\theta_1, \theta_2)$: the first measures the

correlation of one Cooper pair at θ_1 with the other at θ_2, and the second represents the correlation of the momentum (π, π) p-h pair at θ_1 with the other p-h pair at θ_2.

The correlation functions can be seen as response functions of the system to an infinitesimal external field, as shown by Bourbonnais and Caron[16] in one dimension. We will generalize this procedure to two dimensions. To the action $S_{l=0}$ we add the term

$$S\{h\}_{l=0} = \int d\tau \int d\mathbf{q} \int d\theta$$
$$\times \left[\int d\epsilon \mathcal{J}(\epsilon, \theta) \hat{\Delta}_{\mathbf{q}}^{\delta}(\epsilon, \theta; \tau) \right] \bar{h}_{\mathbf{q}}^{\delta}(\theta; \tau) + \text{H.c.}$$
$$(3.13)$$

The external angle dependent fields $\bar{h}_{\mathbf{q}}^{\delta}(\theta; \tau)$ are the source fields coupled to the order-parameter variables of the type δ. The correlation functions (3.10) are obtained as

$$\chi_{l\mathbf{q}}^{\delta}(\theta_1, \theta_2; |\tau_1 - \tau_2|)$$
$$= - \left[\frac{\delta^2 \ln Z}{\delta h_{\mathbf{q}}^{\delta}(\theta_1; \tau_1) \delta \bar{h}_{\mathbf{q}}^{\delta}(\theta_2; \tau_2)} \right]_{h, \Psi_<, \bar{\Psi}_< = 0}.$$
$$(3.14)$$

Setting slow modes to zero means symbolically that we want the response only from the fast modes, as defined in Eq. (3.10). We consider only the static and long-wavelength limit. For that reason we will simply write $\chi(\theta_1, \theta_2)$ instead of $\chi_{\mathbf{q}=0}(\theta_1, \theta_2; i\omega = 0)$ and $h(\theta)$ instead of $h_{\mathbf{q}=0}(\theta; i\omega = 0)$. The correlations with nonzero $\mathbf{q}$ and ω are related to the dynamics of the collective modes, a problem which we do not study in this work.

We now apply the Kadanoff-Wilson-Polchinski formalism to the action containing terms (3.13). The procedure of collecting differential cumulants is analogous to what we explained in Sec. II, but now we treat $S\{h\}$ terms together with the interaction part S_I. To obtain the correlation functions for $h \to 0$, it is sufficient to follow the renormalization of the first two terms in powers of h in the h-dependent part of the effective action. They read

$$S\{h\}_l = \oint d\theta_1 \oint d\theta_2 \left[\int_0^{\Lambda(l)} d\epsilon \mathcal{J}(\epsilon, \theta_1) \hat{\Delta}_{\mathbf{q}}^{\delta}(\epsilon, \theta_1; \tau) \right]$$
$$\times z_l^{\delta}(\theta_1, \theta_2) \bar{h}^{\delta}(\theta_2) + \text{H.c.}$$
$$+ \oint d\theta_1 \oint d\theta_2 \bar{h}^{\delta}(\theta_1) \chi_l^{\delta}(\theta_1, \theta_2) h^{\delta}(\theta_2)$$
$$+ \text{tree terms}\{h\bar{h}\}. \qquad (3.15)$$

The term with $\chi_l^{\delta}(\theta_1, \theta_2)$ contains no electronic variable: it results from the elimination of all outer-shell electrons. From definition (3.14), one can see that $\chi_l^{\delta}(\theta_1, \theta_2)$ is just the susceptibility of type δ. The ''tree terms'' are the terms containing one outer-shell contraction, two slow-electron fields, and fields h and $\bar{h}$. They are illustrated by Fig. 11 for the AF channel. The square symbolizes the effective interaction for
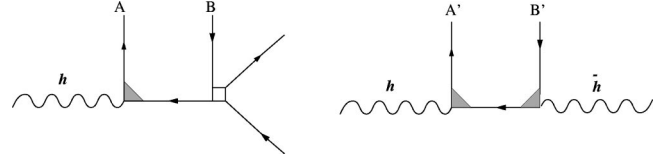
FIG. 11. Tree diagrams containing the source fields for the AF channel.

antiferromagnetism V_l^{AF}. We obtain it from the spin–spin interaction U_σ (see the Appendix) putting the particles 1 and 3 on the opposite sides of the square Fermi surface so that $\mathbf{k}_1 - \mathbf{k}_3 = (\pm \pi, \pm \pi)$ (as in Fig. 10):

$$V_l^{AF}(\theta_1, \theta_2) = -(XU)(\theta_1, \theta_2, \tilde{\theta}_1). \qquad (3.16)$$

$\tilde{\theta}$ is a function of θ such that

$$\mathbf{k}(\theta) - \mathbf{k}(\tilde{\theta}) = (\pi, \pi), \qquad (3.17)$$

$\mathbf{k}$ being on the square Fermi surface. The tree terms for the SC channel are analogous, but with different orientations of the arrows: in the vertex z_l^{SC} both arrows point outward, and in the vertex $\bar{z}_l^{SC}$ both arrows point inward. The corresponding interaction is the familiar effective Cooper amplitude V [Eq. (3.5)]. All ''tree terms'' in Eq. (3.15) are produced by the tree term of the Polchinski equation applied to the action with the $S\{h\}_l$ terms.

The coefficient $z_l^{\delta}(\theta_1, \theta_2)$ is the effective vertex of type δ. Equation (3.13) gives the initial conditions for z,

$$z_{l=0}^{\delta}(\theta_1, \theta_2) = \delta_D(\theta_1 - \theta_2), \qquad (3.18)$$

where δ_D is the Dirac function and, for χ,

$$\chi_{l=0}^{\delta}(\theta_1, \theta_2) = 0. \qquad (3.19)$$

The differential flow of the triangular vertices z_l and of the correlation functions χ is obtained from the loop diagram of the Polchinski equation applied to the tree terms in the action $S\{h\}_l$. For the AF channel, the cumulant with on-shell integration of electrons A and B in Fig. 11 gives contributions to the vertex z_l^{AF}, and the cumulant with electrons A' and B' on the shell contributes to the susceptibility χ_l^{AF}. A similar construction yields the renormalization of the vertex and of the susceptibility for the superconductivity. The resulting diagrams for the differential recursion relations for both channels are shown in Fig. 12.

The corresponding flow equations are written

$$\dot{z}_l^{\delta}(\theta_1, \theta_2) = - \oint d\theta \, z_{l_\delta}^{\delta}(\theta_1, \theta) D_l^{\delta}(\theta) V_{l_\delta}^{\delta}(\theta, \theta_2)$$
$$(3.20)$$

and

$$\dot{\chi}_l^{\delta}(\theta_1, \theta_2) = \oint d\theta \, z_{l_\delta}^{\delta}(\theta_1, \theta) D_l^{\delta}(\theta) z_{l_\delta}^{\delta}(\theta, \theta_2). \quad (3.21)$$

The scales l_{SC} and l_{AF} symbolize the scales l_{pp} and l_{ph} given by expressions (2.22) and (2.23), with the total momentum $\mathbf{q}_{pp} = 0$ and with the momentum transfer $\mathbf{q}_{ph} = (\pi, \pi)$ (antiferromagnetic wave vector):
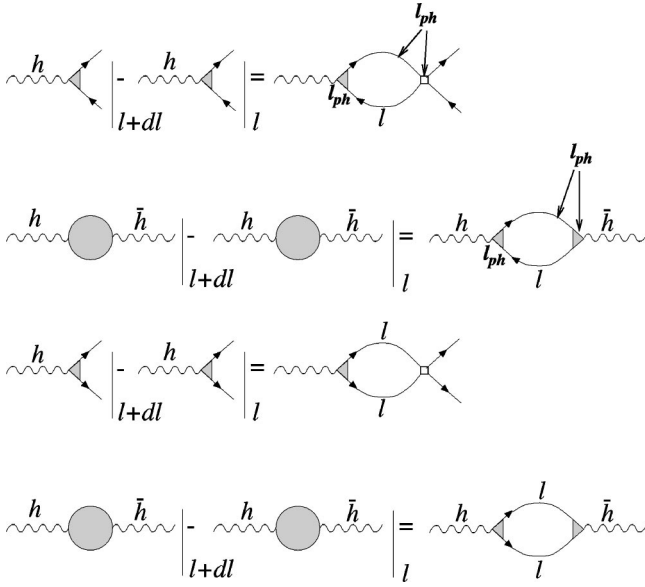
FIG. 12. The recursion relations for the vertices and for the correlation functions of superconducting and antiferromagnetic types.

$$l_\delta = \begin{cases} l_{pp}\big|_{\mathbf{q}_{pp}=0} = l & \text{for } \delta \text{ superconductivity} \\ l_{ph}\big|_{\mathbf{q}_{ph}=(\pi,\pi)} = \ln\dfrac{\Lambda_0}{\Lambda_l + 2|\mu|} & \text{for } \delta \text{ antiferromagnetic.} \end{cases}$$

We see that the renormalization of the antiferromagnetic correlation function is nonlocal in l if the filling is not exactly one-half. The function $D_l^\delta(\theta)$ is

$$D_l^{SC}(\theta) = \frac{1}{2} \sum_{\nu=+,-} \mathcal{J}[\nu\Lambda(l), \theta] \qquad (3.22)$$

for the superconducting channel and

$$D_l^{AF}(\theta) = \frac{1}{2} \frac{\mathcal{J}(-\Lambda(l), \theta)}{1 + |\mu|/\Lambda(l)} \qquad (3.23)$$

for the antiferromagnetic channel, where only the negative shell ($\nu = -1$) contributes to the flow. One sees that $D_l^{AF}(\theta)$ decays exponentially with l for $\Lambda \ll |\mu|$: in the BCS regime the correlation function for antiferromagnetism saturates with increasing l.

From Eqs. (3.20) and (3.21), we see that information about the *symmetry* of the correlations is determined from the symmetry of the effective interactions: functions $D_l^\delta(\theta)$ have a total lattice symmetry, but the interactions $V_l^\delta(\theta, \theta_2)$ can belong to any of the representations of the crystal symmetry group, in our case the D_4 point group. The decomposition of the interaction in terms of all basis functions of all irreducible representations of the D_4 group was discussed in detail in our previous paper.[23] The diagonalization of the correlation functions $\chi_l^\delta(\theta_1, \theta_2)$ gives the final answer about which correlations are dominant in both AF and SC channels. The strength of the dominant correlations is associated wit the maximal eigenvalues, and the corresponding eigenvectors determine the symmetry and the form of the microscopic fluctuating field.

C. Discretization of renormalization-group equations

The interaction U_l that we want to renormalize is a function of three continuous angular variables θ_1, θ_2, and θ_3. The β function given by Eqs. (2.25)–(2.27), (3.6), and (3.7) is a complicated function bilinear in U, and it does not seem possible to find an analytic solution for the flow of the interaction. We thus use numerical method. For that purpose we cut the Brillouin zone in m_i angular (θ) patches, and we assume that the interaction is a function only of the patch indices (i_1, i_2, i_3) of the three angles θ_1, θ_2, and θ_3. After the discretization of the interaction function the differential loops Ξ and Π also become functions of three indices:

$$\Xi\{U, U\}(i_1, i_2, i_3) = \sum_{i=0}^{m_i} B_{pp}(i_1, i_2, i; l)$$
$$\times U_{l_{pp}}(i_1, i_2, i) U_{l_{pp}}(i_3, i_4, i), \qquad (3.24)$$

$$\Pi\{U_1, U_2\}(i_1, i_2, i_3) = \sum_{i=0}^{m_i} B_{ph}(i_1, i_3, i; l) U_{1, l_{ph}}(i_1, i, i_3)$$
$$\times U_{2, l_{ph}}(i_4, i, i_2), \qquad (3.25)$$

with

$$B_{pp}(i_1, i_2, i; l) = \frac{-2}{(2\pi)^2} \sum_{\nu=+,-} \int_{[i]} d\theta \, \mathcal{J}(\nu\Lambda, \theta)$$
$$\times \frac{\Theta(\nu\xi_{\mathbf{k}_\nu - \mathbf{q}_{pp}})\Theta(|\xi_{\mathbf{k}_\nu - \mathbf{q}_{pp}}| - \Lambda)}{1 + \dfrac{\nu}{\Lambda}\xi_{\mathbf{k}_\nu - \mathbf{q}_{pp}}}$$

$$(3.26)$$

and

$$B_{ph}(i_1, i_3, i; l) = \frac{2}{(2\pi)^2} \sum_{\nu=+,-} \int_{[i]} d\theta \, \mathcal{J}(\nu\Lambda, \theta)$$
$$\times \frac{\Theta(-\nu\xi_{\mathbf{k}_\nu + \mathbf{q}_{ph}})\Theta(|\xi_{\mathbf{k}_\nu + \mathbf{q}_{ph}}| - \Lambda)}{1 - \dfrac{\nu}{\Lambda}\xi_{\mathbf{k}_\nu + \mathbf{q}_{ph}}}.$$

$$(3.27)$$

The total momentum and the momentum transfer become discrete variables:

$$\mathbf{q}_{pp} = \mathbf{k}(i_1) + \mathbf{k}(i_2),$$

$$\mathbf{q}_{ph} = \mathbf{k}(i_1) - \mathbf{k}(i_3).$$

The integral $\int_{[i]}$ is over the ith angular sector.

For a given number m_i of patches the number of *coupling constants* is equal to the number of configurations of three indices for all four particles lying on the square Fermi surface. That is a very large number. However because of the symmetry many of the coupling constants are identical. The available symmetries are as follows: (i) The symmetries of the D_4 point group (mirror, $\pi/4$-rotations). (ii) Time inver-

m_i	no. of coupling const.
4	4
8	20
12	47
16	93
20	156
24	244
32	497
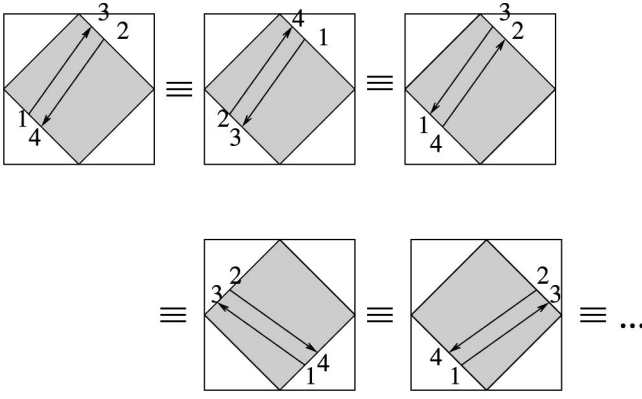
$m_i = 4$	
1	(0000)
2	(0013)
3	(0101)
4	(0110)

$m_i = 8$	
1	(0000)
2	(0015)
3	(0026)
4	(0101)
5	(0110)
6	(0125)
7	(0152)
8	(0202)
9	(0211)
10	(0220)
11	(1111)
12	(1133)
13	(1155)
14	(1313)
15	(1331)
16	(1357)
17	(1375)
18	(1515)
19	(1537)
20	(1551)

FIG. 13. This figure shows how we reduce the number of coupling constants by applying symmetry transformations. The dependence of the number of independent coupling constants on the number of angular patches m_i, and the list of coupling constants for $m_i = 4$ and 8, are also shown.

sion symmetry $\mathcal{T}$, exchanging particles with holes, and vice versa (see the Appendix). (iii) The exchange symmetry, which is allowed to exchange (1,2) and (3,4) particles simultaneously. (iv) The freedom of choice of the points at the edges of the Brillouin zone.

Figure 13 illustrates some of the symmetry operations applied to one of the coupling constants. The same figure shows the relation between the number of patches and the corresponding number of different marginal coupling constants, and the list of the coupling constants for $m_i = 4$ and 8.

The renormalization of the interaction as a function of three angles is now represented by a set of coupled differential equations, one for each coupling constant. In the same way we discretize the correlation functions $\chi_l^\delta(\theta_1, \theta_2)$ and the vertices $z_l^\delta(\theta_1, \theta_2)$. Equations (3.20) and (3.21) become

$$\dot{z}_l^\delta(i_1, i_2) = -\sum_i z_{l_\delta}^\delta(i_1, i) \bar{D}_l^\delta(i) V_{l_\delta}^\delta(i, i_2) \qquad (3.28)$$

and

$$\dot{\chi}_l^\delta(i_1, i_2) = \sum_i z_{l_\delta}^\delta(i_1, i) \bar{D}_l^\delta(i) z_{l_\delta}^\delta(i, i_2), \qquad (3.29)$$
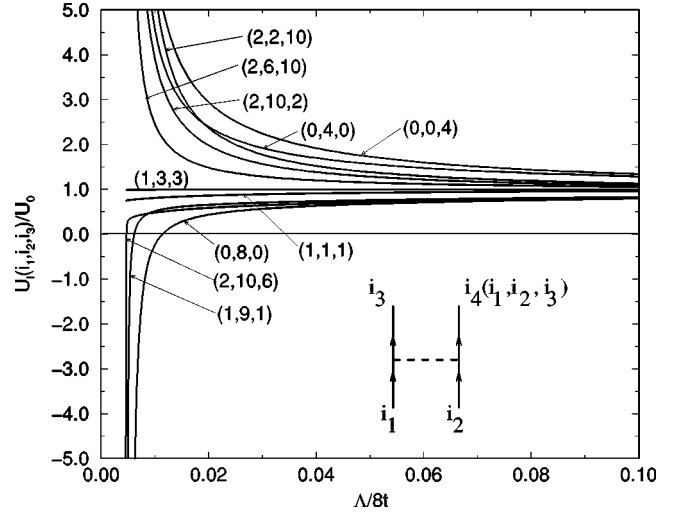
FIG. 14. The flow of a few typical (among 93) scattering amplitudes for a Fermi surface covered by 16 patches, for chemical potential $|\mu| = 8t \exp(-7.8)$ and initial interaction $U = 4t/3$.

with

$$\bar{D}_l^\delta(i) \equiv \int_{[i]} d\theta \, D_l^\delta(\theta). \qquad (3.30)$$

The initial conditions are the same as in the continuous case, provided we replaced the δ function by the Kronecker symbol divided by m_i:

$$\delta_D(\theta - \theta') \rightarrow \delta_{i,i'}/m_i.$$

D. Results and discussion

We have numerically integrated the renormalization equations for all coupling constants and correlation functions, and have analyzed how the results change as functions of the initial interaction U_0 and of the chemical potential μ. We first look at the renormalization flow of the coupling constants. Figure 14 shows the flow of several (among 93) coupling constants for a discretization of $M_i = 16$; the choice of the input parameters is $U_0 = 4t/3$, and $l_\mu \equiv \ln 8t/|\mu| = 7.8$. The divergence occurs at the critical cutoff $\Lambda_c = \Lambda_0 \exp - l_c \approx \Lambda_0 \exp - 5.3$. Approaching this point, some of the coupling constants increase and diverge, while some decrease and, after changing their sign, diverge to $-\infty$. Some do not change significantly upon renormalization and almost do not diverge. In fact, in one-loop renormalization all zero-order marginal processes diverge. The ones that ''almost'' do not diverge are those with a pole strength much weaker than the bare interaction. For example the coupling constant $U(0, m_i/2, 0)$ diverges very strongly to $-\infty$. It is a typical interaction with a singular Cooper channel ($\mathbf{q}_{pp} = 0$) without nesting. Indeed, all coupling constants obeying only the Cooper condition ($\mathbf{q}_{pp} = 0$) and without logarithmic flow in the p-h channel diverge to $-\infty$. This is what we expected since the p-p channel ''pushes'' interactions downward in a repulsive model. However, instead of just decaying to zero, they continue to decrease toward $-\infty$ because the Cooper amplitude obtains *attractive* components from p-h diagrams in, for example, the D-wave channel. Coupling constants with
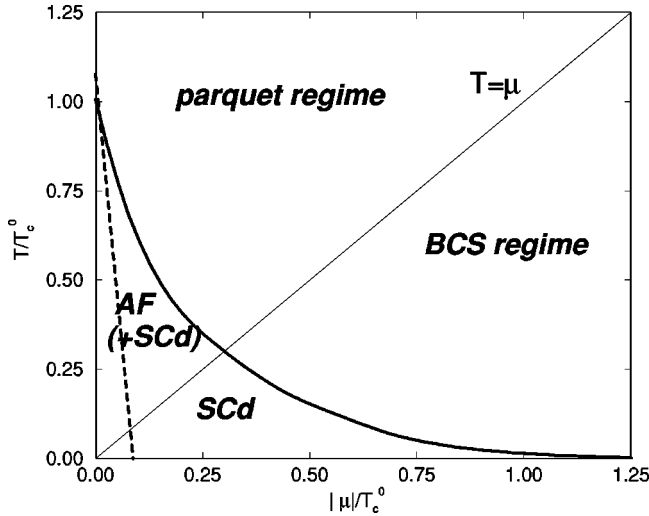
FIG. 15. The phase diagram. The solid line is the critical temperature T_c^{RG}, and the dashed line is the temperature T_c^{MF}.

nesting between particles 1 and 3 or 1 and 4 diverge to $+\infty$. Among the interactions with nesting there are also umklapp processes like $(0,0,4)$ or $(2,2,10)$ in Fig. 14. The processes (almost) without divergence are those without any logarithmic instability either from the nesting or from the Cooper logarithm.

The critical scale l_c depends on the initial interaction and on the chemical potential. We associate the cutoff $\Lambda_0 \exp(-l_c)$ with the critical temperature T_c^{RG}. As we stated in Sec. I, this temperature *is not* a critical temperature for long-range order. Instead, T_c^{RG} should be interpreted as a mean-field-like critical temperature. Figure 15 shows T_c^{RG} as a function of the chemical potential calculated for $m_i = 32$ patches (497 different coupling constants). T_c^{RG} decreases rapidly but never really falls to zero: it becomes exponentially small far from half-filling, the regime analyzed in Ref. 23. Our numerical calculations show that this form is universal if one measures μ in units of the critical temperature at half-filling T_c^0,

$$T_c^{RG} = T_c^0 \times f\left(\frac{|\mu|}{T_c^0}\right), \qquad (3.31)$$

where f is the universal function visible in Fig. 15. Thus T_c depends on the interaction only through $T_c^0 \equiv 8t \exp(-l_c^0)$, where

$$(l_c^0)^2 = C \frac{4t}{U_0}, \qquad (3.32)$$

C being a numerical constant: $C \approx 8.8$. The dashed line in Fig. 15 represents the critical temperature T_c^{MF} that one obtains when taking into account only the last term of Eq. (2.25): $X\beta\{XU, XU\}$. This is the ''renormalization-group'' version of the RPA summation, equivalent to the mean field for the antiferromagnetism. We now see the main difference between the critical temperature in the mean-field approximation and the result obtained with the renormalization group: in the case of weak doping, because of the *destructive* interference between p-p and p-h channels, T_c^{RG} is slightly

reduced with respect to T_c^{MF}. The ratio between the critical scales l_c^{RG} and l_c^{MF} (associated with RG and MF critical temperatures) do not depend on the interaction. Its value at half-filling is $l_c^{MF}/l_c^{RG} = 0.985$, which is not far from the value 0.981 calculated by Dzyaloshinskii and Yakovenko using parquet equations.[20] T_c^{MF} disappears completely at some threshold doping. This means that the physical mechanisms which reduce T_c^{RG} near half-filling enhance T_c^{RG} at higher doping keeping it always nonzero.

The straight line $T = \mu$ is roughly the crossover between the parquet and the BCS regimes. If the instability occurs in the parquet regime, both p-p and p-h correlations are strongly enhanced near T_c^{RG}. On the other hand, in the BCS regime only the p-p correlations are critical. To know which fluctuations are the most important at the instability, we need a renormalization of the correlation functions. However, there is a formal problem related to the fact that we are performing the renormalization at $T = 0$ and associating the cutoff to the temperature: the renormalization equations for the antiferromagnetic vertex (3.28) and the correlation function (3.29) (δ antiferromagnetic) are *retarded* in l of a quantity $l - \ln[\Lambda_0/(\Lambda_l + 2|\mu|)]$. If the interaction V_l^{AF} diverges at $l = l_c$, the divergence of the function χ_l^{AF} will be retarded. Since we cannot go further than $l = l_c$ in the renormalization this divergence cannot be seen in the present formalism. The cure is to work at a finite temperature. In this case one performs the full renormalization, up to $l = \infty$, and the final *fixed-point* correlation functions are the ones at the given temperature. This is the procedure that we use in Sec. IV.

However, in the zero-temperature formalism one can still obtain some idea of what happens with different correlations at $l = l_c$: the finite cutoff divergence of the correlation functions for SC and AF are determined exclusively by the divergence of the effective interactions V_l^{SC} and V_l^{AF}. Furthermore the symmetry of the correlation functions is also brought only by the symmetry of the effective interactions. It is thus reasonable to assume that the dominant eigenvalue of the correlation function is driven mostly by the dominant attractive (negative) eigenvalue of the corresponding effective interaction. From the renormalization of the interaction (the set of coupling constants) we can deduce the flow of the effective interactions V_l^{SC} and V_l^{AF} as given by Eqs. (3.5) and (3.16). The diagonalization is straightforward because both interactions are matrices whose rows and columns are labeled by discretized angular variables. Let us call the most attractive eigenvalues of V_l^{SC} and V_l^{AF}, respectively, V_c^{SC} and V_c^{AF}.

Figure 16 shows the flow of V_c^{SC} and of V_c^{AF} near the critical point as a function of $\ln([\Lambda - T_c^{RG}(\mu)]/4t)$ for several values of the chemical potential. The critical temperature $T_c^{RG}(\mu)$ is adjusted for every value of μ. Solid lines represent the antiferromagnetic interaction V_c^{AF}. The corresponding eigenvector belongs to A_1. It is a standard S wave. The dashed lines represent the flow of V_c^{SC}. Its eigenvector belongs to the B_1 representation ($D_{x^2-y^2}$ wave). Both coupling constants are always enhanced by the renormalization, which means that the correlation functions are always enhanced respectively to their value at $U_0 = 0$. The possibility of the charge-density wave instability is excluded: we have
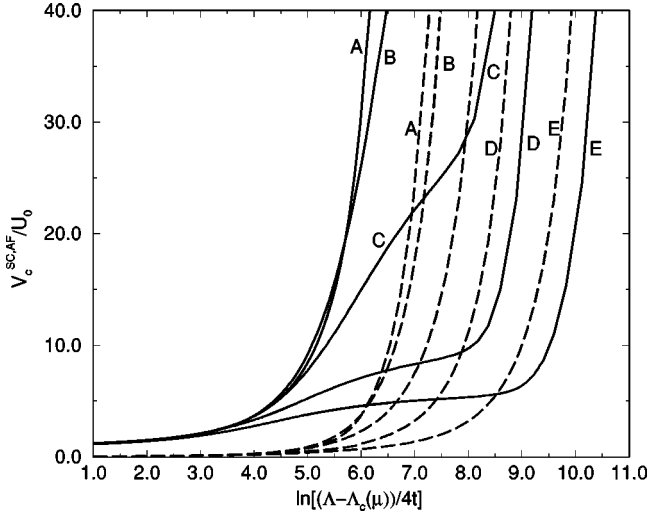
FIG. 16. The flow of V_c^{SC} (dashed line) and of V_c^{AF} (solid line) for $|\mu|/(4t) = 0$ (A), 0.00067 (B), 0.0018 (C), 0.0049 (D), and 0.0081 (E).

checked that all eigenvalues of the charge interactions U_c (see the Appendix) at $2k_F$ decay upon renormalization. The competition between the divergences of V_c^{SC} and V_c^{AF} is clearly visible in the figure. At half-filling the coupling V_c^{AF} diverges faster than V_c^{SC}. As the chemical potential increases, both divergences are weaker but in V_c^{AF} an inversion of the slope is visible. This is the signature of the crossover from the parquet regime to the BCS regime. At half filling this crossover does not exist and the slope of V_c^{AF} is always upwards. The lines labeled by C in the figure correspond to the critical temperature in the parquet regime. However, V_c^{AF} starts to ''feel'' the proximity of the crossover: the critical scale is $l_c = 6.025$ and the crossover occurs at about $l_x \sim l_\mu = 7$. The divergence of V_c^{AF} can still entail the divergence of the antiferromagnetic correlation function because the nesting is still relevant. The Cooper amplitude V_c^{SC} always has an upward slope and diverges at T_c^{RG} because the p-p channel has a logarithmic instability for any doping. Lines D and E are examples of the flow in the BCS regime. After some saturation tendencies, V_c^{AF} still diverges at T_c^{RG}. This divergence is only due to the p-p loop: for a choice of angles θ_1 and θ_2 such that $\theta_2 = \theta_1 + \pi$, it is the function $V^{AF}(\theta_1, \theta_2) = V^{SC}(\theta_1, \tilde{\theta}_1)$ that diverges. The relation between θ_1 and $\tilde{\theta}_1$ is given by Eq. (3.17). The interaction V_c^{AF} is thus driven upwards by the Cooper channel. It has no effect on the correlation function for the antiferromagnetism because its flow has disappeared together with the nesting. This will become visible in Sec. IV, where we calculate the temperature dependence of both correlation functions near the critical temperature.

IV. FINITE-TEMPERATURE RG

In the zero-temperature formalism the flow of different quantities was of physical interest. In the finite-temperature renormalization group, we are interested in the fixed-point value of the correlation functions. The temperature is taken as input parameter. If T is larger than the critical cutoff Λ_c
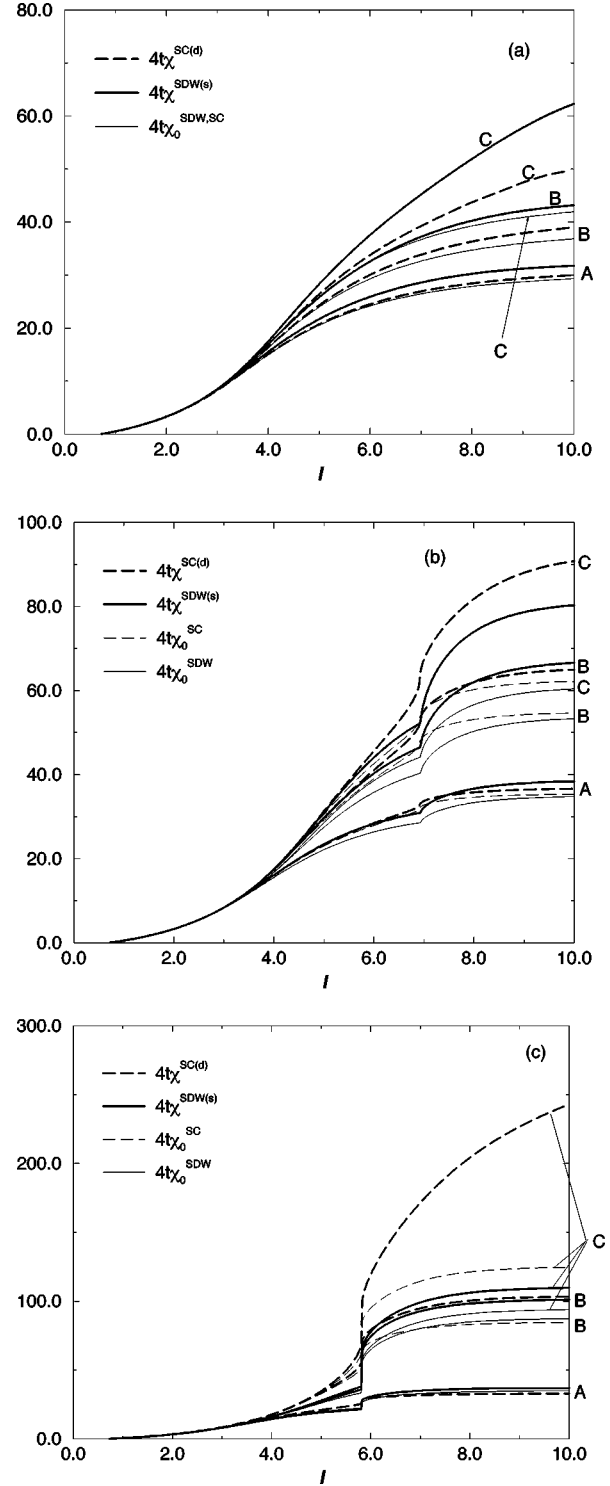
FIG. 17. The flow of the correlation functions with interaction (thick lines) and without interaction (thin lines) (a) at half filling for $T/4t = 0.03$ (A), 0.0204 (B), and 0.0163 (C); (b) at $|\mu|/4t = 0.002$ for $T/4t = 0.0228$ (A), 0.0108 (B), and 0.0086 (C); and (c) at $|\mu|/4t = 0.006$ for $T/4t = 0.03$ (A), 0.006 (B), and 0.0026 (C).

(called T_c^{RG} in Sec. III), the divergence of the renormalization flow will disappear. Consequently we will be able to control the flow all the way down to the fixed point $\Lambda = 0$. In the zero-temperature formalism the effects of the elimination of the slow modes are neglected. At finite temperature all modes are integrated so that contributions of the thermal

electrons are also taken into account. The other advantage of the finite temperature renormalization group is that we can explicitly follow the temperature dependence of the correlation functions for the superconductivity and the antiferromagnetism.

Formally, the finite-temperature procedure is the same as in Sec. III, with the difference that the differential loops Ξ and Π have to be calculated at finite temperature. They now can be written

$$\Xi\{U,U\}(T,\theta_1,\theta_2,\theta_3)$$

$$= \frac{-2}{(2\pi)^2} \sum_{\nu=+,-} \int d\theta\, \mathcal{J}(\nu\Lambda,\theta)$$

$$\times \frac{[1-f(\nu\Lambda)-f(\xi_{\mathbf{k}_\nu-\mathbf{q}_{pp}})]\Theta(|\xi_{\mathbf{k}_\nu-\mathbf{q}_{pp}}|-\Lambda)}{\nu+\frac{1}{\Lambda}\xi_{\mathbf{k}_\nu-\mathbf{q}_{pp}}}$$

$$\times U_{l_{pp}}(\theta_1,\theta_2,\theta)U_{l_{pp}}(\theta_3,\theta_4,\theta), \qquad (4.1)$$

$$\Pi\{U_1,U_2\}(T,\theta_1,\theta_2,\theta_3)$$

$$= \frac{2}{(2\pi)^2} \sum_{\nu=+,-} \int d\theta\, \mathcal{J}(\nu\Lambda,\theta)$$

$$\times \frac{[f(\nu\Lambda)-f(\xi_{\mathbf{k}_\nu+\mathbf{q}_{ph}})]\Theta(|\xi_{\mathbf{k}_\nu+\mathbf{q}_{ph}}|-\Lambda)}{\nu-\frac{1}{\Lambda}\xi_{\mathbf{k}_\nu+\mathbf{q}_{ph}}}$$

$$\times U_{1,l_{ph}}(\theta_1,\theta,\theta_3)U_{2,l_{ph}}(\theta_4,\theta,\theta_2). \qquad (4.2)$$

The function $f(\epsilon)$ is the Fermi distribution at temperature T. The finite-temperature version of the flow equations for the vertices z and for the correlation functions χ are again given by Eqs. (3.20) and (3.21), but with modified D^{SC},

$$D_l^{SC}(T,\theta) = \sum_{\nu=+,-} \mathcal{J}(\nu\Lambda,\theta)\tanh\left(\frac{\nu\Lambda}{2T}\right), \qquad (4.3)$$

and D^{AF},

$$D_l^{AF}(T,\theta)$$

$$= \sum_{\nu=+,-} \mathcal{J}(\nu\Lambda,\theta)$$

$$\times \frac{[f(\nu\Lambda)-f(2|\mu|-\nu\Lambda)]\Theta(|2|\mu|-\nu\Lambda|-\Lambda)}{2\left(\nu-\frac{|\mu|}{\Lambda}\right)}. \qquad (4.4)$$

We see that now both shells $\nu=+$ and $-$ contribute to D_l^{AF} for $\Lambda>|\mu|$, unlike in the zero-temperature case where $\nu=+$ contributions were forbidden by the Fermi distribution. In the discretized version of the flow equations, one calculates Ξ and Π from expressions (3.24) and (3.25), but with

$$B_{pp}(i_1,i_2,i;l,T)$$

$$= \frac{-2}{(2\pi)^2} \sum_{\nu=+,-} \int_{[i]} d\theta\, \mathcal{J}(\nu\Lambda,\theta)$$

$$\times \frac{[1-f(\nu\Lambda)-f(\xi_{\mathbf{k}_\nu-\mathbf{q}_{pp}})]\Theta(|\xi_{\mathbf{k}_\nu-\mathbf{q}_{pp}}|-\Lambda)}{\nu+\frac{1}{\Lambda}\xi_{\mathbf{k}_\nu-\mathbf{q}_{pp}}} \qquad (4.5)$$

and

$$B_{ph}(i_1,i_3,i;l,T)$$

$$= \frac{2}{(2\pi)^2} \sum_{\nu=+,-} \int_{[i]} d\theta\, \mathcal{J}(\nu\Lambda,\theta)$$

$$\times \frac{[f(\nu\Lambda)-f(\xi_{\mathbf{k}_\nu+\mathbf{q}_{ph}})]\Theta(|\xi_{\mathbf{k}_\nu+\mathbf{q}_{ph}}|-\Lambda)}{\nu-\frac{1}{\Lambda}\xi_{\mathbf{k}_\nu+\mathbf{q}_{ph}}}. \qquad (4.6)$$

The equations for finite temperature $z_l^\delta(T,i_1,i_2)$ and $\chi_l^\delta(T,i_1,i_2)$ are Eqs. (3.28) and (3.29) with $D_l^\delta(T,i)$ calculated from Eq. (3.30), but using Eqs. (4.3) and (4.4).

To find each point of the phase diagram, we have to find the fixed-point ($\Lambda\to0$) value of the maximal eigenvalues $\chi_c^\delta(T,l)$ of the correlation functions $\chi_l^\delta(i_1,i_2)$; (δ superconducting and ferromagnetic). This means that the complete renormalization from $l=0$ to $l\to\infty$ has to be done for each temperature.

The flow of the quantities $\chi_c^{SC}(T,l)$ and $\chi_c^{AF}(T,l)$ is shown in Fig. 17 for several temperatures and three different values of the chemical potential. The susceptibilities for the noninteracting ($U=0$) case are also shown. For all calculations the initial interaction was $U_0=4t/3$ and we have cut the Brillouin zone into $m_i=32$ patches. The symmetry of the dominant superconducting correlations is for all cases B_1 (which transforms as $d_{x^2-y^2}$) and the dominant antiferromagnetic correlations have A_1 (s) symmetry. They correspond to the symmetries of the strongest attractive components of the effective interactions $V^{SC,AF}$ found in Sec. III.

Let us concentrate first on Fig. 17(a), that shows the flow at half-filling. The entire flow is in the parquet regime: the nesting is perfect. In the beginning of the flow where $\Lambda_l \gg T$ all correlation functions, bare or with correlations, scale as if the temperature was zero, i.e., like $\ln^2(\Lambda_0/\Lambda)=l^2$. As the cutoff approaches the temperature, the flow starts to saturate. At the same time the effects of the interaction become more and more visible as we decrease the temperature. For all temperatures χ_c^{AF} and χ_c^{SC} are enhanced from their bare values χ_0^{AF} and χ_0^{SC} that are equal at half-filling. As we approach the temperature $T\approx0.016$ from above, the difference between the bare and the interacting cases increases rapidly; this temperature is in fact the critical temperature T_c^{RG} discussed in Sec. III. We have approximated the fixed-point values $\chi_c^{*\delta}(T)$ and $\chi_0^{*\delta}(T)$ of $\chi_c^\delta(T,l)$ and $\chi_0^\delta(T,l)$ with their value for $l=10$ (the corresponding energy Λ_l is much smaller than any physical energy scale). Figure 18(a) shows the temperature dependence of the fixed-point values at half-
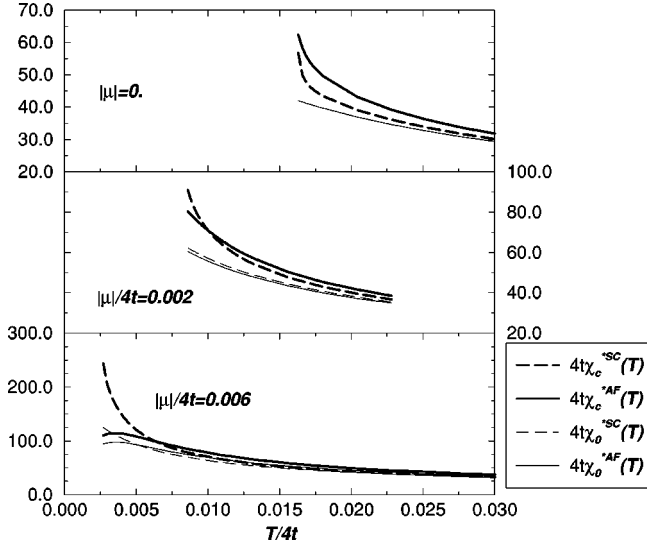
FIG. 18. The temperature dependence of the fixed-point correlation functions for three different values of the chemical potential.

filling. The bare susceptibility scales as $\ln^2(\Lambda_0/T)$. The interaction makes both susceptibilities diverge, but the antiferromagnetic one diverges first.

Now we increase the chemical potential to $|\mu|/4t = 0.002$ [Fig. 17(b)]. The beginning of the flow, where $\Lambda_l \gg |\mu|$, is still square logarithmic. When l becomes close to $l_\mu = 6.9$ the bare antiferromagnetic correlations start to be weaker because we approach the crossover from the parquet to the BCS regime. The nonanalytic point is at $l = l_\mu$; at this point the flow equations (3.28) and (3.29) have a peak because of the van Hove singularity in $D_l^\delta(\theta)$ at $\theta = 0, \pi/2, \pi$, and $3\pi/2$. Again, as we approach the temperature T_c^{RG} the effects of the interaction become stronger and stronger so that the difference between $\chi_c^\delta(T,l)$ and $\chi_0^\delta(T,l)$ increases more and more. The temperature dependence of the fixed-point values for all correlation functions for the present case are shown in Fig. 18(b). The instability temperature is $T_c^{RG}/4t \approx 0.0075$, which is higher than $|\mu|/4t = 0.002$. This means that the instability is still in the parquet regime, but not too deeply: the proximity of the crossover already affects the antiferromagnetic correlations, which start to lose their strength with respect to the superconducting correlations near the instability. However, both are still strongly enhanced and their flow is dominated by the parquet part ($l < l_\mu$) for all temperatures $T > T_c^{RG}$.

Let us further increase the chemical potential to $|\mu|/4t = 0.006$ [Fig. 17(c)]. The flow of the antiferromagnetic correlations saturates in the BCS regime ($l > l_\mu = 5.8$), but both correlation functions SC and AF remain enhanced from their bare values. In the temperature dependence of their fixed point values [Fig. 18(c)], one sees that only the superconducting instability is possible. The temperature T_c^{RG} is lower than the chemical potential, i.e., the instability is in the BCS regime, in which the p-h part of the flow is negligible. The antiferromagnetic susceptibility even starts to decrease with the temperature when $T \lesssim \mu$. This happens because we do not adjust the wave vector of the spin-density wave (SDW) to the best nesting (incommensurate SDW) but we keep it for simplicity at (π, π). Nothing drastic would happen even if

we have taken small deviations of the best nesting wave vector from (π, π): the susceptibility would saturate as the temperature decreases because the differential p-h bubble decays in the BCS regime *at any wave vector* with positive power of Λ.

The universal function $f(|\mu|/T_c^0)$ [Eq. (3.31)], which determines the dependence of T_c^{RG} on the chemical potential, is practically the same as the one obtained in the zero-temperature formalism. The final phase diagram is the one in Fig. 15. At half-filling the antiferromagnetic fluctuations are dominant over the superconducting ones, but both correlation functions diverge at $T = T_c^{RG}$. Upon doping the antiferromagnetic correlations lose their strength while the superconducting correlations remain strongly divergent. The divergence of AF correlation functions is completely suppressed if $T = T_c^{RG}$ is in the BCS regime.

V. CONCLUSION

We have formulated the exact Kadanoff-Wilson-Polchinski (KWP) renormalization group for a general problem of interacting fermions on a two-dimensional lattice. In principle the generalization to higher dimensions is trivial. The procedure of the KWP renormalization scheme is to integrate out successively the degrees of freedom starting from high energies, and to follow the renormalization of *all* terms in the effective action. We parametrize the renormalization by a high-energy cutoff $\Lambda \equiv \Lambda_0 \exp(-l)$ determining the ring $\pm \Lambda$ around the Fermi surface. In order to take the whole Brillouin zone into account, the cutoff Λ is taken to be equal to the bandwidth ($\Lambda_0 = \mathcal{B}$) at the beginning of the renormalization ($l = 0$). As one proceeds with the mode elimination, vertices of all orders are created. To follow the exact renormalization of the effective action we need to know the flow (the dependence on l) of all vertices. The Polchinski equation [Eqs. (2.16) and (2.17), and Fig. 3] determines the differential flow of all vertices as *functions* of energies and momenta. In principle the fixed point solution ($l \to \infty$) of this equation gives us the exact connected Green functions of the model.[32,33] Clearly, the exact integration of Polchinski equation is impossible and for concrete calculations we have to truncate the effective action.

The truncation at the sextic term (at the three-particle interaction term) generates the one-loop renormalization group for the two-body interaction. The truncated effective action is given by expression (2.21). Its renormalization is determined by the flow equation for the two-body interaction and for the self-energy. The flow equation for the interaction U_l is made of all one-loop diagrams bilinear in U_l as shown in Fig. 4 and by Eq. (2.25). Note that U_l is renormalized as a function of three energy momenta (the fourth is conserved), i.e., this is a *functional* renormalization group. The β function (2.25) contains the contributions from the p-p (β_{pp}) and p-h diagrams (β_{ph}). The first term is called the BCS contribution in the literature, the next three terms are the zero sound (ZS) contribution, and the last term is the ZS$'$ contribution to the differential flow. The flow equation for the interaction is not local in l, as one can see from Eqs. (2.28) and (2.29) for differential p-p and p-h bubbles: at some step l of the renormalization, U_l is renormalized by the values of U at former steps $l_{pp}(\mathbf{k}, \mathbf{k}_1, \mathbf{k}_2)$ and $l_{ph}(\mathbf{k}, \mathbf{k}_1, \mathbf{k}_3)$. This non-

locality is the price we have to pay if we want to keep all contributions, logarithmic or not, that renormalize the interaction. In this way one takes correctly into account, for example, the p-h flow because of the imperfectly nested Fermi surface. The standard (local) Wilsonian RG,[31] that takes into account only dominant logarithmic diagrams (those with $l = l_{pp} = l_{ph}$), can give useful results only for the perfectly nested (but not square) Fermi surfaces or the Fermi surfaces far from being nested, so that the p-h part is negligible.

We have applied the one-loop renormalization group to the Hubbard model on a square lattice near half-filling. The interaction function U that we renormalize is dependent on the angular (θ) position of three momenta on the square Fermi surface (the fourth one is conserved). All radial momentum dependencies and energy (ω) dependencies are irrelevant to the Fermi-liquid scaling. It is important that we allow variables θ of the interacting particles to be anywhere on the square Fermi surface, and not only in the configurations which give perfect nesting or zero total momentum (see Fig. 7). This means that we do not limit ourselves to the leading logarithmic parts of the flow, but that we take all non-logarithmic contributions into account.

From the explicit scale dependence of the differential flow for U we see two renormalization regimes (see Fig. 9). In the first regime, $\Lambda_l > |\mu|$. We call it the parquet regime because both p-p and p-h contributions are important. The other regime exists in the non-half-filled case when $\Lambda_l < |\mu|$. There only p-p loops have a strong logarithmic flow, while the p-h part decays to zero. We call this regime the BCS regime. The effective phase space $[|\xi_0(\mathbf{k})| < \Lambda]$ in the parquet regime is open so that the nesting is relevant (see Fig. 2), while in the BCS regime the phase space is a closed regular ring of degrees of freedom around the Fermi surface so that perfect nesting is impossible (see Fig. 6). The flow in the parquet regime is characterized by a strong coupling between the p-p and p-h channels of renormalization. This coupling comes into play over the interactions that have a strong flow from both p-p and p-h diagrams. For the case of a (nearly) square Fermi surface these are all interactions between electrons from opposite sheets of the Fermi surface.

The leading correlations in the Hubbard model are expected to be antiferromagnetic and/or superconducting. To give a precise answer to this question, we use the Kadanoff-Wilson-Polchinski procedure to construct the renormalization-group equations for the *angle-resolved* correlation functions $\chi_l^{AF}(\theta_1, \theta_2)$ and $\chi_l^{SC}(\theta_1, \theta_2)$ for antiferromagnetism and superconductivity, defined by Eq. (3.10). At a given step $\Lambda(l)$ of the renormalization these correlation functions measure the linear response of the electrons outside the shell $\pm \Lambda$ around the Fermi surface. We take the static long-wave limit. The renormalization equation for $\chi_l^{AF,SC}$ is Eq. (3.21). The renormalization of the correlation functions depends on the renormalization of the vertices $z^{AF,SC}$ [Eq. (3.20)]. Furthermore, from Eqs. (3.20) and (3.21) one sees that the flows of the susceptibilities and of the vertices depend on the flows of the corresponding *effective interactions* V_l^{SC} and V_l^{AF}, given by Eqs. (3.5) and (3.16), respectively.

The flow equations for the interaction U_l [Eq. (2.25)], for the vertices $z_l^{SC,AF}$ [Eq. (3.20)], and for the correlation functions $\chi_l^{SC,AF}$ [Eq. (3.21)] can be integrated numerically if we

discretize their θ dependence. The coupling function is then approximated by a set of coupling constants. The vertices and correlation functions become discrete matrices. Using physical and geometrical symmetries we reduce the number of coupling constants to a set of the independent ones (see Fig. 13). The functional renormalization-group equations become a set of equations, one for each coupling constant and for each matrix element of $z_l^{SC,AF}$ and $\chi_l^{SC,AF}$.

We have solved the renormalization equations for up to $m_i = 32$ angular patches. The typical flow of the coupling constants is shown in Fig. 14. There is a critical scale for which coupling constants diverge. We associate it with the critical temperature T_c^{RG}. Its dependence on the chemical potential is shown in Fig. 15 (solid line) together with the RPA result (dashed line). At the line $T_c^{RG}(\mu)$ the electronic correlations are strongly enhanced. The type and form of the corresponding microscopical fluctuating fields are given by the dominating eigenvalues (and their eigenvectors) of the correlation matrices $\chi_l^{SC,AF}$. These are determined by the dominant attractive eigenvalues V_c^{SC} and V_c^{AF} of the effective interactions. For all values of the chemical potential studied in this work, the eigenvalue V_c^{SC} corresponds to $d_{x^2-y^2}$ (or B_1) singlet superconductivity while V_c^{AF} is an s wave (A_1 representation). The flow of the interactions V_c^{SC} and V_c^{AF} in the vicinity of the critical point $\Lambda = T_c^{RG}$ is shown in Fig. 16. At half-filling, V_c^{AF} is dominant. Upon doping, the divergence of V_c^{AF} loses its strength and the divergence of V_c^{SC} becomes dominant.

To determine the dominant fluctuations near T_c^{RG} more precisely, we have done one further step in the renormalization-group formalism: we have introduced the temperature explicitly into the flow equations. In this formalism the cutoff Λ no longer has the physical meaning of the effective temperature. At a given temperature T the physical information is contained in the fixed point ($\Lambda \to 0$) of the correlation functions. This extension of the formalism was necessary because in the zero-temperature procedure it was not possible to have the divergence of χ_l^{AF} at the same scale l_c as the divergence of the coupling V^{AF}: for any nonzero chemical potential the flow of χ_l^{AF} has a finite retardation in l [see Eqs. (3.20) and (3.21)]. Thus χ_l^{AF} diverges later, at $l > l_c$. In the finite-temperature formalism χ_l^{AF}, χ_l^{SC}, V_l^{AF}, and V_l^{SC} all diverge at the same temperature. The price of this is that for each temperature we have to integrate the complete flow all the way from $l = 0$ to $l = \infty$, and to follow how the result changes with the temperature.

The flow of the dominant eigenvalues of χ_l^{AF} and χ_l^{SC} at a few different values of the temperature is shown in Fig. 17 for three different values of the chemical potential. Both correlation functions are always enhanced with respect to their bare ($U = 0$) values. The temperature dependence of the fixed point correlation functions is shown in Fig. 18. The critical temperature T_c^{RG} found by the finite-temperature method is practically the same as the one found by zero-temperature calculations, but now we are able to follow explicitly the enhancement of the correlations of both types in the vicinity of the instability. It is clearly visible how the doping favors superconductivity and how the divergence of χ^{*AF} is completely suppressed if the instability is in the BCS

regime, i.e., if $T_c^{RG} < |\mu|$. This result justifies the phase diagram in Fig. 15.

In the low-doping regime, both correlations are strongly enhanced, and the low-temperature phase can in principle be a mixture of both (quasi-)long-range orders, with the superconducting component falling to zero at half-filling. The instability is in the parquet regime: the critical fluctuations are a mixture of two fluctuating channels and cannot be treated by an effective mean-field theory like BCS or RPA theories. In other words, the parquet regime is deeply non-Migdalian, so that the vertex corrections are as important as the p-p loops. The vertex corrections can no longer be seen as small, but have to be taken at all orders, just as the p-p diagrams, and together with other p-h loops.

The situation is less complicated in the BCS regime. There, a low-energy effective action can be constructed so that only the p-p diagrams contribute to the instability while the p-h parts (antiferromagnetic tendencies) are irrelevant. The attractive d-wave component of the Cooper amplitude in the LEEA is due to the higher energies ($\epsilon > |\mu|$), where the p-h diagrams are important. In the BCS regime only superconductivity is possible as a low-temperature order.

As we are considering a two-dimensional system, one should be careful about the interpretation of T_c: in the case of magnetism, this indicates the onset of well-defined finite-range correlations. For weak interactions, this is typically a very well-defined crossover.[36] In the case of pairing T_c^{RG} can be identified with the onset of quasi-long-range order. Furthermore, the line between AF(SCd) and SC phases in Fig. 15 is only partially determined in our calculations: we only know that at temperature near T_c^{RG}, this line is close to the crossover line $T = |\mu|$, but at lower temperatures we cannot say anything about its position.

It is difficult to discuss the experimental results from the point of view of our phase diagram. First of all, the one-loop renormalization group is a weak coupling perturbative method, while the interactions in the copper-oxide superconductors are moderate to strong. For that reason our phase diagram can be compared to the experiments only qualitatively. Furthermore, in our calculations we have neglected self-energy corrections, which are given in Polchinski's formalism by Hartree-Fock-like terms with renormalized ω- and $\mathbf{q}$-dependent vertices [Eq. (2.30)]. The broadening and redistribution of the spectral weight of the quasiparticles is then determined by the dynamics of the vertex, which is irrelevant and therefore neglected. One should however notice that at the two-loop level self-energy effects become important, as known from the one-dimensional case.[15] In that sense, our T_c^{RG} should be understood as a temperature where the effects of interactions start to change strongly not only the two-particle correlations, but the single-particle properties as well. For that reason it seems natural to associate the temperature T_c^{RG} with the crossover temperature T_{co} found in the cuprates. The parquet regime would then correspond roughly to the underdoped situation, and the BCS regime to the overdoped regime.

The ''phase'' AF(SCd) corresponds then to the antiferromagnetism and to the pseudogap regime: the antiferromagnetic correlations and the localization tendencies there are accompanied more and more with superconducting correla-

tions as we approach the crossover line $T = |\mu|$. We expect that the critical temperatures for antiferromagnetism and superconductivity in this regime are lower than T_c^{RG}, because of the self-energy corrections. In other words, at temperature T_c^{RG} in the parquet regime, the local antiferromagnetic moments and d-wave singlets are created with finite correlation lengths. This gives rise to pseudogaps in both spin and charge responses, together with the precursors of both antiferromagnetism and d-wave superconductivity. The absence of the long-range order between superconductivity and antiferromagnetism in the phase diagram of cuprates is perhaps due to the fact that both types of fluctuations are strong. That is the central idea of the $SO(5)$ models[42] for the high-T_c superconductivity. In that language our T_c^{RG} plays the role of the mean-field critical temperature for the $SO(5)$ field.

In the BCS regime only the superconducting fluctuations are critical. We thus associate the phase SCd with the overdoped regime. From large-N arguments[31,23] we know that the self-energy corrections disappear as T_c/t if the Fermi surface is not nested. This is the case in the BCS regime where the nesting processes are irrelevant. Consequently, in this regime T_c^{RG} is the BCS-like critical temperature. In two dimensions no long-range order is possible, but a Kosterlitz-Thouless transition for superconductivity exists. The corresponding critical temperature T_{KT} is close to the mean-field one, T_c^{RG}:[17]

$$\frac{T_c^{RG} - T_{KT}}{T_c^{RG}} \approx \frac{T_c^{RG}}{E_F} \ll 1. \tag{5.1}$$

This means that in the BCS regime a phase transition exists near T_c^{RG} even in the absence of interplane coupling (third dimension).

Experimentally, in the overdoped regime the crossover temperature T_{co} is equal to the critical temperature for the superconductivity. Independently of the mechanisms for the phase transition, Kosterlitz-Thouless or interplane hopping, this existence of one single characteristic temperature which is the critical temperature is a reason to believe that the critical temperature in the overdoped regime is very close to the mean-field critical temperature. Finally, mean-field arguments[43] suggest that one expects an incommensurate SDW (ICSDW) only in the BCS regime, and only where the imperfect nesting is still strong, i.e., not far from the crossover $T = |\mu|$. However, the precision of our calculation (we cut the Brillouin zone into up to 32 θ patches) is not sufficient to check whether a magnetic correlation function diverges at some incommensurate wave vector. In any case, the incommensurate SDW and d superconductivity are not in competition because they appear at different places on the Fermi surface: SCd in the corners and the ICSDW in the flat parts; one thus expects their coexistence.

Altogether, the phase diagram in Fig. 15 has important similarities to the experimental phase diagrams. The one–loop renormalization group, taking into account electron–electron and electron–hole processes on the same footing, reveals the essence of the physics of a doped half-filled band of correlated electrons.

ACKNOWLEDGMENTS

APPENDIX: INTERACTION $U(1,2,3)$ AND ITS SYMMETRIES

The most general spin-rotation-invariant interaction term can be written in several ways. One way is in terms of charge-charge and spin-spin interactions,

$$U_c(K_1,K_2,K_3)\bar{C}(K_2,K_4)C(K_3,K_1)$$

$$+ U_\sigma(K_1,K_2,K_3)\bar{\mathbf{S}}(K_2,K_4)\cdot\mathbf{S}(K_3,K_1), \quad (A1)$$

where C and S_i are

$$C(K_3,K_1)\equiv\sum_\sigma \bar{\Psi}_{\sigma K_3}\Psi_{\sigma K_1},$$

$$S_i(K_3,K_1)=\sum_{\sigma\sigma'} \bar{\Psi}_{\sigma K_3}\sigma^i_{\sigma\sigma'}\Psi_{\sigma' K_1}. \quad (A2)$$

The summation over all three energy-momentum vectors (K_1,K_2,K_3) is assumed and $K_4=K_1+K_2-K_3$. On the other hand, the interaction can also be written as a sum of one term with equal $(\sigma=\sigma')$ spin quantum numbers and one with opposite $(\sigma=-\sigma')$ spin quantum numbers, with corresponding coupling functions $U_\parallel(K_1,K_2,K_3)$ and $U_\perp(K_1,K_2,K_3)$,

$$U_\parallel(K_1,K_2,K_3)\bar{\Psi}_{\sigma K_3}\bar{\Psi}_{\sigma K_4}\Psi_{\sigma K_2}\Psi_{\sigma K_1}$$

$$+ U_\perp(K_1,K_2,K_3)\bar{\Psi}_{\sigma K_3}\bar{\Psi}_{-\sigma K_4}\Psi_{-\sigma K_2}\Psi_{\sigma K_1}, \quad (A3)$$

with the summation over spin indices assumed. Spin-rotation invariance allows us to write the interaction part of the action as a sum of the singlet $(|\vec{\sigma}+\vec{\sigma}'|=0)$ and triplet $(|\vec{\sigma}+\vec{\sigma}'|=\sqrt{2})$ parts,

$$\bar{s}(K_4,K_3)U^S(K_1,K_2,K_3)s(K_2,K_1)$$

$$+ \bar{t}_\mu(K_4,K_3)U^A(K_1,K_2,K_3)t_\mu(K_2,K_1), \quad (A4)$$

where s and t_μ are the variables of annihilation of the singlet and triplet states:

$$s(K_2,K_1)\equiv\frac{1}{\sqrt{2}}\sum_\sigma \sigma\Psi_{\sigma K_2}\Psi_{-\sigma K_1}, \quad (A5)$$

$$t_0(K_2,K_1)\equiv\frac{1}{\sqrt{2}}\sum_\sigma \Psi_{\sigma K_2}\Psi_{-\sigma K_1},$$

$$t_{\pm 1}(K_2,K_1)\equiv\Psi_{\uparrow,\downarrow K_2}\Psi_{\uparrow,\downarrow K_1}. \quad (A6)$$

All coupling functions in Eqs. (A2)–(A4) possess a symmetry related to momentum exchange and time inversion. If $\mathcal{F}(K_1,K_2,K_3,K_4)$ is a coupling function, two exchange operators can be defined as

$$X\mathcal{F}(K_1,K_2,K_3,K_4)\equiv\mathcal{F}(K_2,K_1,K_3,K_4) \quad (A7)$$

and

$$\bar{X}\mathcal{F}(K_1,K_2,K_3,K_4)\equiv\mathcal{F}(K_1,K_2,K_4,K_3). \quad (A8)$$

The time inversion operator $\mathcal{T}$ is

$$\mathcal{T}\mathcal{F}(K_1,K_2,K_3,K_4)\equiv\mathcal{F}(K_3,K_4,K_1,K_2). \quad (A9)$$

The symmetries of the coupling function are the time inversion symmetry

$$\mathcal{T}\mathcal{F}=\mathcal{F} \quad (A10)$$

and the exchange symmetry

$$X\bar{X}\mathcal{F}=\mathcal{F}. \quad (A11)$$

Both symmetries can be easily checked for coupling functions in expression (A3). We will see that all other couplings can be derived from $U_\perp$ only, and have the same symmetry properties upon X and $\mathcal{T}$ operations. It is easy to see that $\bar{X}\mathcal{F}=X\mathcal{F}$ if $\mathcal{T}\mathcal{F}=\mathcal{F}$: the exchanging of particles 1 and 2 or particles 3 and 4 is equivalent.

We want now to find the relations between the six coupling functions in Eqs. (A2)–(A4). Using the Pauli principle one obtains

$$U_\parallel=U_c+U_\sigma, \quad (A12)$$

$$U_\perp=U_c-U_\sigma-2XU_\sigma. \quad (A13)$$

Let us suppose U_c and U_σ to be two independent functions. We can write them in the forms

$$U_c=\frac{1}{4}(2-X)U_1+U_2, \quad (A14)$$

$$U_\sigma=-\frac{X}{4}U_1. \quad (A15)$$

If we now *choose* $U_1=U_\perp$ it follows from Eq. (A13) that $U_2=0$. This means that the most general interaction can be written in terms of a single function $U_\perp$, without losing generality. The function $U_\parallel$ is also contained in $U_\perp$. That is, from two equal-spin electrons one can build only a triplet state (antisymmetric under X), so that

$$U_\parallel=U^A, \quad (A16)$$

while

$$U_\perp=U^A+U^S, \quad (A17)$$

containing the singlet and the triplet interactions. U^A and U^S can be seen as the antisymmetric and symmetric parts of the same function. This function is simply $U_\perp$.

We see that all coupling functions are contained in $U_\perp$, which we call simply U or U_l to make its scale dependence explicit. One thus has

$$U_c = \frac{1}{4}(2-X)U, \quad U_\sigma = -\frac{X}{4}U, \qquad \text{(A18)}$$

$$U^A = U_\parallel = \frac{1}{2}(1-X)U, \quad U^S = \frac{1}{2}(1+X)U. \qquad \text{(A19)}$$

The effective coupling function for the renormalization of the AF correlation function [Eq. (3.16)] is obtained from the spin coupling

$$V_l^{AF}(\theta_1,\theta_2) = 4U_{\sigma l}(\theta_1,\theta_2,\tilde{\theta}_1), \qquad \text{(A20)}$$

where we take only the θ dependence of the coupling functions into account. The angle $\tilde{\theta}$ is related to the angle θ in such a way that the momentum difference between the particles $\mathbf{k}(\theta)$ and $\mathbf{k}(\tilde{\theta})$ is the perfect nesting vector ($\pm\pi$, $\pm\pi$). The coupling function for the charge density wave (CDW) at $\mathbf{q}=(\pi,\pi)$ would be

$$V_l^{CDW}(\theta_1,\theta_2) = 4U_{cl}(\theta_1,\theta_2,\tilde{\theta}_1). \qquad \text{(A21)}$$

---

*Present address: Laboratoire de Physique Théorique et Hautes Energies, Universités Paris VI Pierre et Marie Curie – Paris VII Denis Diderot, 2 Place Jussieu, 75252 Paris Cédex 05, France.

†Deceased.

[1] For a recent review see, for example, M. B. Maple, cond-mat/9802202 (unpublished).

[2] See for example, D. Pines and Ph. Nozieres, *Quantum Liquids* (Benjamin, New York, 1966), and the original works of L. D. Landau, Zh. Éksp. Teor. Fiz. **30**, 1058 (1956) [Sov. Phys. JETP **3**, 920 (1956)]; **32**, 59 (1957) [**5**, 101 (1957)]; **35**, 97 (1958) [**8**, 70 (1959)].

[3] D. A. Wollman, D. J. Van Harlingen, J. Giapintzakis, and D. M. Ginsberg, Phys. Rev. Lett. **74**, 797 (1995); J. R. Kirtley, C. C. Tsuei, J. Z. Sun, C. C. Chi, L. S. Yujahnes, A. Gupta, M. Rupp, and M. B. Ketchen, Nature (London) **373**, 225 (1995); R. C. Dynes, Solid State Commun. **92**, 53 (1994); W. N. Hardy, D. A. Bonn, D. C. Morgan, R. X. Liang, and K. Zhang, Phys. Rev. Lett. **70**, 3999 (1993); J. A. Martindale, S. E. Barrett, K. E. O'Hara, C. P. Slichter, W. C. Lee, and D. M. Ginsberg, Phys. Rev. B **47**, 9155 (1993); D. J. Scalapino, Phys. Rep. **250**, 329 (1995).

[4] Z.-X. Shen, W. E. Spicer, D. M. King, D. S. Dessau, and B. O. Wells, Science **267**, 343 (1995).

[5] M. R. Norman, M. Randeria, J. C. Campuzano, T. Yokoya, T. Takeuchi, T. Takehashi, T. Mochiku, K. Kadowaki, P. Guptasarma, and D. G. Hinks, Nature (London) **392**, 157 (1998).

[6] Ch. Renner, B. Revaz, J.-Y. Genoud, K. Kadowaki, and O. Fischer, Phys. Rev. Lett. **80**, 149 (1998).

[7] H. Alloul, Bull. Am. Phys. Soc. **34**, 663 (1989); H. Alloul, T. Ohno, and P. Mendels, Phys. Rev. Lett. **63**, 1700 (1989); W. W. Warren, Jr., R. E. Walstedt, G. F. Brennert, R. J. Cava, R. Tycko, R. F. Bell, and G. Dabbagh, *ibid.* **62**, 1193 (1989); C. Berthier, M. Horvatić, P. Carretta, Y. Berthier, P. Ségransan, J. A. Gillet, T. Auler, and J. Y. Henry, Physica C **235**, 67 (1994); G. V. M. Williams, J. L. Tallon, E. M. Haines, R. Michalak, and R. Dupree, Phys. Rev. Lett. **78**, 721 (1997).

[8] R. J. Birgeneau, Y. Endoh, K. Kakurai, Y. Hidaka, T. Muramaki, M. A. Kastner, T. R. Thurston, G. Shirane, and K. Yamada, Phys. Rev. B **39**, 2868 (1989); J. Rossat-Mignod, L. P. Regnault, C. Vettier, P. Burlet, J. Y. Henry, and G. Lapertot, Physica B **169**, 58 (1991).

[9] D. Jérome and H. J. Schulz, Adv. Phys. **31**, 299 (1982); D. Jérome, in *Organic Conductors*, edited by J. P. Farges (Dekker, New York, 1994), p. 405.

[10] J. E. Schirber, D. L. Overmyer, K. D. Carlson, J. M. Williams, A.

M. Kini, H. Hau Wang, H. A. Charlier, B. J. Love, D. M. Watkins, and G. A. Yaconi, Phys. Rev. B **44**, 4666 (1991); H. Mayaffre, P. Wzietek, C. Lenoir, D. Jérome, and P. Batail, Europhys. Lett. **28**, 205 (1994); K. Miyagawa, A. Kawamoto, Y. Nakazawa, and K. Kanoda, Phys. Rev. Lett. **75**, 1174 (1995); K. Kanoda, Physica C **282-287**, 299 (1997).

[11] J. Moser, M. Gabay, P. Auban-Senzier, D. Jérome, K. Bechgaard, and J. M. Fabre, Eur. Phys. J. B **1**, 39 (1998).

[12] N. F. Berk and J. R. Schrieffer, Phys. Rev. Lett. **17**, 433 (1966); Phys. Rev. B **30**, 1408 (1966).

[13] D. J. Scalapino, Phys. Rep. **250**, 329 (1995).

[14] N. E. Bickers, D. J. Scalapino, and S. R. White, Phys. Rev. Lett. **62**, 961 (1989).

[15] V. J. Emery, in *Highly Conducting One Dimensional Solids*, edited by J. T. Devreese, R. P. Evrard, and V. E. Van Doren (Plenum, New York, 1979), p. 247; J. Solyom, Adv. Phys. **28**, 201 (1979).

[16] C. Bourbonnais and L. G. Caron, Int. J. Mod. Phys. B **5**, 1033 (1991).

[17] H. J. Schulz, Europhys. Lett. **4**, 609 (1987).

[18] P. Lederer, G. Montambaux, and D. Poilblanc, J. Phys. (Paris) **48**, 1613 (1987).

[19] I. E. Dzyaloshinskii, Zh. Éksp. Teor. Fiz. **93**, 1487 (1987) [Sov. Phys. JETP **66**, 848 (1988)].

[20] I. E. Dzyaloshinskii and V. M. Yakovenko, Zh. Éksp. Teor. Fiz. **94**, 344 (1988) [Sov. Phys. JETP **67**, 844 (1988)].

[21] A. T. Zheleznyak, V. M. Yakovenko, and I. E. Dzyaloshinskii, Phys. Rev. B **55**, 3200 (1997).

[22] F. Vistulo de Abreu and B. Douçot, Europhys. Lett. **38**, 533 (1997).

[23] D. Zanchi and H. J. Schulz, Phys. Rev. B **54**, 9509 (1996).

[24] D. Zanchi and H. J. Schulz, Z. Phys. B: Condens. Matter **103**, 339 (1997).

[25] J. Gonzalez, F. Guinea, and M. A. H. Vozmediano, Phys. Rev. Lett. **79**, 3514 (1997).

[26] J. Ruvalds, C. T. Rieck, S. Tewari, J. Thoma, and A. Virosztek, Phys. Rev. B **51**, 3797 (1995).

[27] H.-J. Kwon, Phys. Rev. B **55**, 5988 (1997).

[28] Hsiu-Hau Lin, Leon Balents, and Matthew P. A. Fisher, Phys. Rev. B **56**, 6569 (1997).

[29] W. Fettes and I. Morgestern, cond-mat/9801227 (unpublished).

[30] Shiwei Zhang, J. Carlson, and J. E. Gubernatis, Phys. Rev. Lett. **78**, 4486 (1997).

[31] R. Shankar, Rev. Mod. Phys. **66**, 129 (1994).

[32] J. Polchinski, Nucl. Phys. B **231**, 269 (1984).

[33] Tim R. Morris, Int. J. Mod. Phys. A **9**, 2411 (1994).

[34] M. Salmhofer, Commun. Math. Phys. **194**, 249 (1998).

[35] See for example: P. M. Chaikin, J. Phys. I **6**, 1875 (1996), and references therein.

[36] H. J. Schulz, Phys. Rev. B **39**, 2940 (1989).

[37] D. Zanchi and H. J. Schulz, Europhys. Lett. **44**, 235 (1998).

[38] J. W. Negele and H. Orland, *Quantum Many-Particle Physics* (Addison-Wesley, Reading, MA, 1988).

[39] E. Fradkin, *Field Theories of Condensed Matter Systems* (Addison-Wesley, Reading, MA, 1991).

[40] S. Weinberg, Nucl. Phys. B **413**, 567 (1994).

[41] D. Zanchi (unpublished).

[42] S.-C. Zhang, Science **275**, 1089 (1997).

[43] D. Zanchi, Ph.D. thesis, Université Paris-Sud, 1996.